This article has been accepted for publication in IEEE Transactions on Wireless Communications. This is the author's version which has not been fully edited and content may change prior to final publication. Citation information: DOI 10.1109/TWC.2024.3417713

Precoding for Multi-Cell ISAC: from Coordinated Beamforming to Coordinated Multipoint and Bi-Static Sensing

Nithin Babu, *Member, IEEE*, Christos Masouros, *Fellow, IEEE*, Constantinos B. Papadias, *Fellow, IEEE*, and Yonina C. Eldar, *Fellow, IEEE*.

***Abstract*—This paper proposes a framework for designing robust precoders for a multi-input single-output (MISO) system that performs integrated sensing and communication (ISAC) across multiple cells and users. We use Cramer-Rao-Bound (CRB) to measure the sensing performance and derive its expressions for two multi-cell scenarios, namely coordinated beamforming (CBF) and coordinated multi-point (CoMP). In the CBF scheme, a BS shares channel state information (CSI) and estimates target parameters using monostatic sensing. In contrast, a BS in the CoMP scheme shares the CSI and data, allowing bistatic sensing through inter-cell reflection. We consider both block-level (BL) and symbol-level (SL) precoding schemes for both the multi-cell scenarios that are robust to channel state estimation errors. The formulated optimization problems to minimize the CRB in estimating the parameters of a target and maximize the minimum communication signal-to-interference-plus-noise-ratio (SINR) while satisfying a given total transmit power budget are non-convex. We tackle the non-convexity using a combination of semidefinite relaxation (SDR) and alternating optimization (AO) techniques. Simulations suggest that neglecting the inter-cell reflection and communication links degrades the performance of an ISAC system. The CoMP scenario employing SL precoding performs the best, whereas the BL precoding applied in the CBF scenario produces relatively high estimation error for a given minimum SINR value.**

***Index Terms*—ISAC, Precoder, Cramer-Rao bound, CoMP, CBF.**

I. Introduction

Integrated sensing and communication (ISAC) has been identified as an enabler for next-generation wireless networks to augment communication services with sensing for emerging applications spanning connected vehicles, remote healthcare, smart homes, and more [1], [2]. The availability of large bandwidth, multiple antennas, and dense deployment of 5G-Advanced and 6G networks enable high-resolution radio sensing capability [3]. ISAC has been recognized as one of the key enablers for 6G by the standardization bodies such as the International Telecommunication Union (ITU) and Third Generation Partnership Project (3GPP) [4] [5]. Having sensing and communication capabilities mutually benefits both systems: sensing can be used by the communication system to understand the environment better and enhance, for instance, interference management and beamforming, whereas the connected network infrastructure enables coordinated sensing at an unprecedented scale.

Numerous works have considered designing optimal transmit waveforms/precoders to improve a single-cell ISAC system's sensing and communication performance [6]–[20]. However, the dense deployment of next-generation small-cell BSs causes the signals transmitted from a BS to its users to affect the sensing and communication performance of neighbouring BSs. When the BSs use the same time and frequency resources to serve users, a user experiences intra-cell interference by the signals intended for other users in the same cell and inter-cell interference (ICI) due to co-channel signal leakage from the neighbouring BSs, reducing the received SINR. The work in [21] discusses various resource allocation schemes and precoder designs to improve the received SINR for a communication-only multi-cell system by suppressing interference. In multi-cell ISAC, a notable difference lies in the fact that while the communication aspect is often limited by interference, multi-static sensing is not necessarily interference-limited. For ISAC, in addition to this, inter-cell reflections (ICR) will be received by a BS from its target due to the signal transmitted from the neighbouring BSs. The received power through ICR can degrade target parameter estimation if the BS is unaware of the data transmitted from the neighbouring BS. This emphasizes the need for coordination among BSs to effectively manage inter-cell communication and sensing links.

The ISAC BSs can coordinate at different levels through coordinated beamforming (CBF) and coordinated multipoint (CoMP) schemes, similar to the communication-only multi-cell system. In an ISAC CBF scheme, a single BS serves a disjoint set of users and estimates its target's parameters through mono-static sensing. Here, the signal power received through the inter-cell links negatively affects the sensing and communication performances. Hence, each BS selects a transmit strategy jointly with other BSs to minimize the ICI and ICR using the globally shared CSI obtained from the users via feedback channels. Conversely, a user is served by all the BSs in an ISAC CoMP scenario, thereby improving the received

For the purpose of open access, the author has applied a Creative Commons Attribution (CC BY) licence to any Author Accepted Manuscript version arising. This work was supported in part by the Engineering and Physical Sciences Research Council under Project EP/S028455/1.

N. Babu and C. Masouros are with the Department of EE, UCL (e-mail: n.babu@ucl.ac.uk, c.masouros@ucl.ac.uk).

C. B. Papadias is with Research, Technology and Innovation Network (RTIN), Alba, The American College of Greece, Greece (e-mail: cpapadias@acg.edu).

Y. C. Eldar is with the Faculty of Mathematics and Computer-Science, Weizmann Institute of Science, Rehovot, Israel (e-mail: yonina.eldar@weizmann.ac.il.)

This article has been accepted for publication in IEEE Transactions on Wireless Communications. This is the author's version which has not been fully edited and content may change prior to final publication. Citation information: DOI 10.1109/TWC.2024.3417713

communication SINR at the user. Since the CoMP scheme shares the user data to be transmitted and the CSI globally among the BSs through a high bandwidth backhaul network, the additional power received through ICR and ICI links enhances estimation accuracy and communication SINR at the expense of increased coordination overhead. In particular, ICR enables bistatic sensing.

Each of these multi-cell scenarios can employ either of two existing precoding strategies that differ in how they deal with the co-channel interference experienced by a user: a) block-level precoding (BLP) [21] and b) symbol-level precoding (SLP) [22]. Conventional precoding, also called BLP, designs precoders for a set of users to transmit a given block of symbols. It treats the interference experienced by a user as a harmful element, whereas constructive interference (CI)-based precoding, also called SLP, uses the signal power received through the instantaneous interference to aid the received communication SINR. The SLP technique exploits knowledge of both CSI and downlink data to be transmitted at the BS to ensure the received symbol at a user falls within the constructive region of the signal constellation [23]. Considering the SLP in the CoMP scheme, each BS can utilize both the intra-cell and inter-cell interference to enhance the received signal power. Conversely, the SLP in the CBF scheme can only utilize the intra-cell interference due to the non-availability of the user data from the neighbouring BSs. The design of the optimal precoders for both coordination schemes depends on the available CSI at the BSs and the users. In practice, CSI is prone to errors necessitating that the designed precoders exhibit robustness to potential CSI uncertainties.

Multi-cell ISAC setups with various combinations of CBF and CoMP schemes have been considered in [24]–[33]. The work in [24] and [25] consider orthogonal transmission among BSs, whereas [26] uses an additional BS as the receiver to enable bi-static sensing and hence does not consider the inter-cell interference links. [27] considers a multi-static scenario where one BS transmits signals to one vehicle, and the echoes are captured by several other BSs for sensing purposes. The paper [28] presents a resource allocation strategy for ISAC in distributed antenna networks, demonstrating significant energy savings and operational efficiency through a novel alternating optimization algorithm. The authors of [29] propose a multi-static architecture in coordinated multi-cell networks for ISAC, featuring an alternating optimization algorithm to optimize transmit and receive beamforming, thereby reducing self-interference and enhancing quality of service. The study in [30] considers CoMP mode to serve a set of users while detecting a target. Here, the transmitter employs distinct sensing and communication signals, allowing for modeling the interference between them. The authors of [31] model multi-cell ISAC interference considering 3 BSs operating in CBF mode where the users are considered as targets. [32] models the inter-user and inter-subsystem interference. In [33], the BSs serve the users in the CBF mode and neglect the inter-cell reflection links. The work in [26], [28]–[30] consider BLP design to achieve various objectives spanning minimizing energy consumption [28], beampattern mismatch error [29] or total transmit power [30] to maximizing the minimum communication SINR [26] subject to radar and or communication constraints. [31] employs a collaborative SLP to mitigate mutual interference in a 3-cell ISAC system and minimize the total transmit power.

A. Main Contributions and Paper Organization

The existing multi-cell ISAC works consider no uncertainty in CSI. Moreover, the work in [24]–[33] employ either orthogonal schemes or CoMP for serving the users, and the sensing model follows the properties of CBF in which the reflections from other targets are considered interference. The proposed sensing models do not capture the property that the reflections from other targets can aid or degrade the sensing depending on the coordination level among the BSs. Furthermore, the sensing performance is quantified using radar SINR value. Explicit optimization of estimation performance metrics has not been considered in [24]–[33]. We considered this aspect in our previous work [34] while deriving the CRB expression for estimating the azimuth angle of a target in a multi-cell ISAC setup. Subsequently, this expression is utilized to design block-level precoders that optimize a weighted combination of sensing and communication metrics without considering channel state uncertainty. It is important to note that the derived CRB expression becomes invalid when dealing with scenarios involving more than one unknown parameter per target or multiple targets per cell. Recall that the precoding design should be robust to CSI uncertainties. The work in [35] designed robust symbol-level precoders for a multi-cell communication system that minimizes the total transmission power without considering the sensing capability. Even though the problem formulations in the aforementioned works consider multi-cell ISAC scenarios, a relative system performance analysis under different levels of coordination amongst BSs spanning from CBF to CoMP in the presence of channel state estimation error has not been investigated. To the best of our knowledge, explicit optimization of a weighted combination of the estimation error and communication performance metrics under CSI uncertainty has not been considered in the context of a multi-cell ISAC network. Our main contributions are:

- We propose a robust precoder design framework to minimize the target parameter estimation error variance and maximize the minimum communication SINR experienced by a user in a multi-cell multi-user MIMO ISAC system under CSI uncertainty.
- We consider two multi-cell scenarios, CBF and CoMP, and extend the corresponding CRB expressions in [34] to multiple parameters (location and complex amplitudes) per target. The important distinction between the two cooperation modes in terms of sensing is that in the CRB, the adjacent BSs' signals act as interference to the monostatic sensing of the serving BS, while in CoMP, the same signals can be used as an additional source of bi-static sensing.
- The derived CRB expressions are then utilized to formulate optimization problems that jointly minimize the CRB value and maximize the minimum communication SINR value subject to a total transmit power budget.

This article has been accepted for publication in IEEE Transactions on Wireless Communications. This is the author's version which has not been fully edited and content may change prior to final publication. Citation information: DOI 10.1109/TWC.2024.3417713

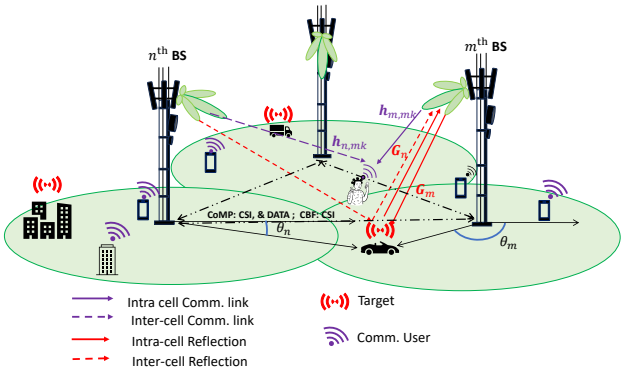

Fig. 1: Diagram of a multi-cell ISAC system, illustrating intra-cell and inter-cell communication links and reflections between BSs, communication users, and targets.

The formulations consider block-level and symbol-level precoding techniques for the CBF and CoMP scenarios.
- We solve all the non-convex optimization problems using a combination of the semidefinite relaxation (SDR) and alternating optimization (AO) methods.
- Finally, we compare the sensing and communication performances of all the considered precoder design schemes through simulations.

The remaining content of the paper is organized as follows: in Section II, we explain the system model and derive the CRB expressions for the CBF and CoMP multi-cell scenarios. Section III and Section IV discuss the block-level and symbol-level robust precoding schemes for the considered multi-cell scenarios. Finally, in Section VI, we present our main findings through numerical evaluation, and the paper is concluded in Section VII.

Notations: Matrices, vectors, and scalars are denoted by bold uppercase, lowercase, and normal font letters, respectively. We use $\mathrm{tr}()$, $()^{\mathrm{T}}$, $()^{\mathrm{H}}$, and $()^*$ to represent trace operation, transpose, Hermitian transpose, and the complex conjugate of the matrices or vectors. The real and imaginary parts of $\mathbf{x}$ are represented as $\mathbf{x}^{\mathrm{R}}$ and $\mathbf{x}^{\mathrm{I}}$, respectively, and $\|\|$ denotes the l_2 norm. We represent an $N \times N$ null matrix and an $N \times N$ identity matrix as $\mathbf{0}_N$ and $\mathbf{I}_N$, respectively. Additionally, $\vec{0}_N$ denotes an $N \times 1$ null vector.

II. System Model

We consider a multi-cell multi-input single-output (MISO) ISAC system with J cells and K single-antenna users per cell. As shown in Fig. 1, in addition to the users, each cell has a target and a BS with a uniform linear array (ULA) of N_{tx} transmit antennas spaced at $\lambda/2$ distance, where λ is the wavelength. The BS is also equipped with a $\lambda/2$-spaced receive ULA of N_{rx} elements for sensing and isolated from the transmit antenna elements. Moreover, the BSs are interconnected through optical cables to synchronize and exchange information.

A. Communication Model and Performance Metric

For the communication service, we aim to maximize the minimum SINR value experienced by a user in a cell. Recall that the corresponding SINR expressions vary depending on the BSs' coordination level (CBF or CoMP) and precoding mode, BLP or SLP, and are detailed in the following. The proposed algorithm requires the channel state information (CSI) to be available at the BS and the users. We consider the system operating in time division duplexing (TDD) mode so that the downlink CSI can be derived from the uplink channel observations based on the received uplink sounding reference signal (SRS) transmitted by the users. Additionally, each user employs a simple equalizer for the composite channel $\mathbf{h}^{\mathrm{T}}\mathbf{w}$, where $\mathbf{h}$ is the communication channel from the serving BS and $\mathbf{w}$ is the precoding vector.

1) Coordinated Beamforming: Let U_{mk} represent the k^{th} user of the m^{th} cell. In practice, the CSI is imperfectly known at the BS. Let the CSI uncertainty be limited within the spherical set $\mathcal{E}_{mk} = \{\mathbf{e}_{mk} : \|\mathbf{e}_{mk}\|^2 \leq \delta^2\}$ [22]. Then, the actual CSI, $\tilde{\mathbf{h}}_{n,mk}$, from the n^{th} BS to U_{mk} is the sum of the observed CSI, denoted as $\{\mathbf{h}_{n,mk}\}$, and $\mathbf{e}_{mk}$:

$$\tilde{\mathbf{h}}_{n,mk} = \mathbf{h}_{n,mk} + \mathbf{e}_{mk},\ \forall U_{mk}. \tag{1}$$

Let the m^{th} BS transmits the symbol matrix $\mathbf{X}_m = [\mathbf{x}_{m1}, \mathbf{x}_{m2}, ..., \mathbf{x}_{mL}] = \mathbf{W}_m\mathbf{S}_m \in \mathcal{C}^{N_{\mathrm{tx}} \times L}$, where $\mathbf{W}_m = [\mathbf{w}_{m1}, \mathbf{w}_{m2}, ..., \mathbf{w}_{mK}]\ \forall\ m \in \{1, 2, .., J\}$ are the dual-functional beamforming matrices to be designed, with $L > N_{\mathrm{tx}}$ being the length of the radar pulse/ communication frame. Here, $\mathbf{S}_m \in \mathcal{C}^{K \times L}$ is the orthogonal data stream transmitted to K users of the m^{th} BS: $(1/L)\mathbf{S}_m\mathbf{S}_m^{\mathrm{H}} = \mathbf{I}_K$. Then the received signal at U_{mk} is expressed as

$$\mathbf{y}_{mk}^{\mathrm{C}} = \tilde{\mathbf{h}}_{m,mk}^{\mathrm{T}}\mathbf{X}_m + \sum_{n \neq m}^{J} \tilde{\mathbf{h}}_{n,mk}^{\mathrm{T}}\mathbf{X}_n + \mathbf{z}_{mk}^{\mathrm{C}}, \tag{2}$$

where $\mathbf{z}_{mk}^{\mathrm{C}} \in \mathcal{C}^{1 \times L}$ is an AWGN noise vector with variance of each entry being σ_{C}^2. Since no data is shared among the BSs in CBF mode, the first term in the RHS of (2) contains the useful signal and intra-cell interference from the users of the same cell, whereas the second term represents the inter-cell interference from the neighbouring cells. In a multi-carrier system, for example, based on orthogonal frequency-division multiplexing (OFDM), the input–output model (2) could describe one of the subcarriers.

2) Coordinated Multipoint: Since the BSs share the user data and the CSI in the CoMP mode, the $J \cdot K$ users in the multi-cell ISAC system can be considered to be served by a virtual single-cell BS with $N = J \cdot N_{\mathrm{tx}}$ antennas. In this scenario, the precoder design occurs at a designated base station serving as the central node. The resulting precoder matrices are then shared with the respective base stations through optical cables. Let U_k for $k \in \{1, 2, \ldots, J \cdot K\}$ represent the k^{th} user of the virtual single-cell system. Note that U_k for $k \in \{K \cdot (m-1)+1, \ldots, K \cdot m\}$ represents K users of the m^{th} BS. Let $\tilde{\mathbf{h}}_k \in \mathcal{C}^{N \times 1}$ be the actual channel vector from all the BSs to U_k represented as

$$\tilde{\mathbf{h}}_k = \mathbf{h}_k + \mathbf{e}_k, \tag{3}$$

This article has been accepted for publication in IEEE Transactions on Wireless Communications. This is the author's version which has not been fully edited and content may change prior to final publication. Citation information: DOI 10.1109/TWC.2024.3417713

where $\mathbf{e}_k \in \mathcal{E}_k = \{\mathbf{e}_k : \|\mathbf{e}_k\|^2 \leq J\delta^2\}$. The received signal at U_k is expressed as

$$\mathbf{y}_k^{\mathrm{C}} = \tilde{\mathbf{h}}_k^{\mathrm{T}}\mathbf{X} + \mathbf{z}_k^{\mathrm{C}}, \tag{4}$$

where $\mathbf{X} = [\mathbf{X}_1; \mathbf{X}_2, ...; \mathbf{X}_J] \in \mathcal{C}^{N\times L}$ is the concatenated symbol matrix available at each BS and $\mathbf{z}_k^{\mathrm{C}} \in \mathcal{C}^{1\times L}$ is an AWGN noise vector with variance of each entry being σ_{C}^2. Since intra-cell and inter-cell interference are treated differently by BLP and SLP, we will present the corresponding SINR expressions in the respective sections.

B. Sensing Model and Performance Metric

As shown in Fig. 1, the BSs transmit simultaneously, and each BS receives its echo signal and multiple echo signals from the neighbouring BSs due to ICR; we consider the dominant path among the ICR paths and the signal power received through the weaker paths is included in the noise term. Hence, the resulting echo signal received by the m^{th} BS from its target is given as

$$\mathbf{Y}_m^{\mathrm{I}} = \mathbf{G}_m\mathbf{X}_m + \underbrace{\sum_{n\neq m}^{J} \mathbf{G}_n\mathbf{X}_n}_{\mathrm{ICR}} + \mathbf{Z}_m^{\mathrm{R}}, \tag{5}$$

where $\mathbf{G}_n = \alpha_n\mathbf{a}_m\mathbf{v}_n^{\mathrm{T}}\ \forall m, n = \{1, 2, .., J\} \equiv \mathcal{J}$, is the target response matrix at the m^{th} BS due to the transmission from the n^{th} BS in which $\mathbf{a}_m$ and $\mathbf{v}_n$ are the array response vectors in the directions at the angle-of-arrival θ_m and the angle of departure θ_n, respectively. Here, α_n represents the complex amplitude of the received signal due to pathloss and the radar cross section of the target and $\mathbf{Z}_m^{\mathrm{R}} \in \mathbb{C}^{N_{\mathrm{rx}}\times L}$ is an additive white Gaussian noise (AWGN) vector with the variance of each entry being σ_{R}^2. Equation (5) assumes that all the neighbouring BSs have a line-of-sight (LoS) link to the m^{th} BS's target. The first term on the right-hand side (RHS) of (5) is the mono-static intra-cell reflection due to the signal vector from the same BS, whereas the second term represents ICR due to the signals from the remaining BSs. Note that when $J = 1$, (5) reduces to the sensing model proposed in [11]. Furthermore, the transmit antennas at the BS are conventionally down-tilted, resulting in negligible BS-BS interference received through the side lobes of the transmit beampattern [36], and hence in (5), we neglect the direct interference link between the BSs. Note that (5) applies to scenarios where users necessitate simultaneous sensing and communication services. In such instances, $\{\mathbf{G}_n\}$ include LoS channels to the users.

1) Sensing Performance Metric: We assume the target parameter estimation happens locally in the CBF and CoMP modes. The sensing process aims to estimate the target parameters using the received echo signal samples $\mathbf{Y}_m^{\mathrm{I}}$. We aim to minimize the variance of the error in the parameter estimation. For an unbiased estimator, the error variance is lower bounded by the CRB given by the inverse of the Fisher information matrix (FIM). In general, not all the unknowns need to be estimated. Let $\boldsymbol{\theta}_{m,*}$ be the set of parameters of interest, and $\boldsymbol{\eta}_{m,*}$ represents the nuisance parameters which are of no interest but present in the received echo signal. Hence, the FIM can be represented as

$$\mathbf{F}_{m,*} = \begin{bmatrix} \mathbf{F}_{\boldsymbol{\theta}_{m,*}\boldsymbol{\theta}_{m,*}} & \mathbf{F}_{\boldsymbol{\theta}_{m,*}\boldsymbol{\eta}_{m,*}} \\ \mathbf{F}^{\mathrm{T}}_{\boldsymbol{\theta}_{m,*}\boldsymbol{\eta}_{m,*}} & \mathbf{F}_{\boldsymbol{\eta}_{m,*}\boldsymbol{\eta}_{m,*}} \end{bmatrix}, \tag{6}$$

where $\mathbf{F}_{\boldsymbol{\theta}_{m,*}\boldsymbol{\theta}_{m,*}}$, $\mathbf{F}_{\boldsymbol{\theta}_{m,*}\boldsymbol{\eta}_{m,*}}$ and $\mathbf{F}_{\boldsymbol{\eta}_{m,*}\boldsymbol{\eta}_{m,*}}$ are the block matrices. The element at the l^{th} row and the p^{th} column of $\mathbf{F}_{m,*}$ can be calculated by [37],

$$F_{lp} = \mathrm{tr}\left(\frac{d\boldsymbol{\mu}_{m,*}^{\mathrm{H}}}{d\zeta_{ml}}\mathbf{C}_{m,*}^{-1}\frac{d\boldsymbol{\mu}_{m,*}}{d\zeta_{mp}}\right), \tag{7}$$

where $\zeta_{ml}, \zeta_{mp} \in \{\boldsymbol{\theta}_{m,*}, \boldsymbol{\eta}_{m,*}\}$. Equation (7) is derived from the observation that the received echo signal at the m^{th} BS is a multi-variate Gaussian random variable with mean $\boldsymbol{\mu}_{m,*}$ and covariance matrix $\mathbf{C}_{m,*}$. The entries of $\boldsymbol{\theta}_{m,*}$,$\boldsymbol{\eta}_{m,*}$ $\boldsymbol{\mu}_{m,*}$ and $\mathbf{C}_{m,*}$ depend on whether the BSs are operating in the CBF or the CoMP mode, whose corresponding expressions are derived in the following propositions by extending the CRB derivation in [37] to a multi-cell ISAC scenario.

2) Coordinated Beamforming for Mono-Static Sensing: In the case of CBF, ICR acts as an interference term to the serving BS's mono-static sensing since $\{\mathbf{X}_n\}$ is unknown to BS m. Therefore, from Eq. (5),

$$\boldsymbol{\mu}_{m,\mathrm{cbf}} = \mathbf{G}_m\mathbf{X}_m, \tag{8}$$

$$\mathbf{C}_{m,\mathrm{cbf}} = L\sum_{n\neq m}^{J} \mathbf{G}_n\mathbf{W}_n\mathbf{W}_n^{\mathrm{H}}\mathbf{G}_n^{\mathrm{H}} + \sigma_{\mathrm{R}}^2\mathbf{I}_{N_{\mathrm{rx}}}. \tag{9}$$

Here, the set of unknown parameters is $\{\theta_m, \alpha_m^{\mathrm{R}}, \alpha_m^{\mathrm{I}}\}$. In this work, we consider each BS needs to estimate its' target's azimuth angle. Hence $\theta_{m,\mathrm{cbf}} = \theta_m$ and $\boldsymbol{\eta}_{m,\mathrm{cbf}} = \{\alpha_m^{\mathrm{R}}, \alpha_m^{\mathrm{I}}\}$. Consequently, the FIM will be a 3×3 matrix given by [1]

$$\mathbf{F}_{m,\mathrm{cbf}} = 2\begin{bmatrix} F^{\mathrm{R}}_{\theta_m\theta_m} & \mathbf{f}_{\theta_m\boldsymbol{\eta}_{m,\mathrm{cbf}}} \\ \mathbf{f}^{\mathrm{T}}_{\theta_m\boldsymbol{\eta}_{m,\mathrm{cbf}}} & \mathbf{F}_{\boldsymbol{\eta}_{m,\mathrm{cbf}}\boldsymbol{\eta}_{m,\mathrm{cbf}}} \end{bmatrix}, \tag{10}$$

whose elements can be calculated using Proposition 1. Additionally, when $\boldsymbol{\zeta}_{ml} = \{\theta_m\}$, (7) represents the Fisher information value derived in [34].

Proposition 1. *The entries of* $\mathbf{F}_{m,\mathrm{cbf}}$ *are computed as*

$$\mathbf{f}_{\theta_m\boldsymbol{\eta}_{m,\mathrm{cbf}}} = [F^{\mathrm{R}}_{\theta_m\alpha_m} - F^{\mathrm{I}}_{\theta_m\alpha_m}], \tag{11}$$

$$\mathbf{F}_{\boldsymbol{\eta}_{m,\mathrm{cbf}}\boldsymbol{\eta}_{m,\mathrm{cbf}}} = \begin{bmatrix} F^{\mathrm{R}}_{\alpha_m\alpha_m} & -F^{\mathrm{I}}_{\alpha_m\alpha_m} \\ -F^{\mathrm{I}}_{\alpha_m\alpha_m} & F^{\mathrm{R}}_{\alpha_m\alpha_m} \end{bmatrix}, \tag{12}$$

[1]The extension to multiple targets and multiple parameters can be done using (10) of [37].

This article has been accepted for publication in IEEE Transactions on Wireless Communications. This is the author's version which has not been fully edited and content may change prior to final publication. Citation information: DOI 10.1109/TWC.2024.3417713

with $F_{\theta_m\theta_m}$ and the elements of $\mathbf{f}_{\theta_m\boldsymbol{\eta}_{m,\mathrm{cbf}}}$ and $\mathbf{F}_{\boldsymbol{\eta}_{m,\mathrm{cbf}}\boldsymbol{\eta}_{m,\mathrm{cbf}}}$ determined using the following equations:

$$\begin{aligned}\frac{1}{L\alpha_m^2}F_{\theta_m\theta_m} &= \dot{\mathbf{a}}_m^{\mathrm{H}}\mathbf{C}_{m,\mathrm{cbf}}^{-1}\dot{\mathbf{a}}_m\cdot\mathbf{v}_m^{\mathrm{H}}\mathbf{R}_{\mathbf{X}_m}^{*}\mathbf{v}_m\\ &+\dot{\mathbf{a}}_m^{\mathrm{H}}\mathbf{C}_{m,\mathrm{cbf}}^{-1}\mathbf{a}_m\cdot\mathbf{v}_m^{\mathrm{H}}\mathbf{R}_{\mathbf{X}_m}^{*}\dot{\mathbf{v}}_m\\ &+\mathbf{a}_m^{\mathrm{H}}\mathbf{C}_{m,\mathrm{cbf}}^{-1}\dot{\mathbf{a}}_m\cdot\dot{\mathbf{v}}_m^{\mathrm{H}}\mathbf{R}_{\mathbf{X}_m}^{*}\mathbf{v}_m\\ &+\mathbf{a}_m^{\mathrm{H}}\mathbf{C}_{m,\mathrm{cbf}}^{-1}\mathbf{a}_m\cdot\dot{\mathbf{v}}_m^{\mathrm{H}}\mathbf{R}_{\mathbf{X}_m}^{*}\dot{\mathbf{v}}_m, \qquad (13)\\ \frac{1}{L\alpha_m^{*}}F_{\theta_m\alpha_m} &= \dot{\mathbf{a}}_m^{\mathrm{H}}\mathbf{C}_{m,\mathrm{cbf}}^{-1}\mathbf{a}_m\cdot\mathbf{v}_m^{\mathrm{H}}\mathbf{R}_{\mathbf{X}_m}^{*}\mathbf{v}_m\\ &+\mathbf{a}_m^{\mathrm{H}}\mathbf{C}_{m,\mathrm{cbf}}^{-1}\mathbf{a}_m\cdot\dot{\mathbf{v}}_m^{\mathrm{H}}\mathbf{R}_{\mathbf{X}_m}^{*}\mathbf{v}_m, \qquad (14)\\ \frac{1}{L}F_{\alpha_m\alpha_m} &= \mathbf{a}_m^{\mathrm{H}}\mathbf{C}_{m,\mathrm{cbf}}^{-1}\mathbf{a}_m\cdot\mathbf{v}_m^{\mathrm{H}}\mathbf{R}_{\mathbf{X}_m}^{*}\mathbf{v}_m, \qquad (15)\end{aligned}$$

where, $\mathbf{R}_{\mathbf{X}_m}=\frac{1}{L}\mathbf{X}_m\mathbf{X}_m^{\mathrm{H}}=\mathbf{W}_m\mathbf{W}_m^{\mathrm{H}}=\sum_{k=1}^{K}\mathbf{w}_{mk}\mathbf{w}_{mk}^{\mathrm{H}}=\sum_{k=1}^{K}\mathbf{W}_{mk}$. Here, the derivatives of $\mathbf{a}_m$ and $\mathbf{v}_m$ with respect to θ_m are denoted by $\dot{\mathbf{a}}_m$ and $\dot{\mathbf{v}}_m$, respectively.

Proof. In CBF, as no data is shared between the BSs, the m^{th} BS knows only the data symbol matrix $\mathbf{X}_m$. Using the definitions of $\mathbf{G}_m$, we have

$$\frac{d\boldsymbol{\mu}_{m,\mathrm{cbf}}}{d\theta_m}=\left(\alpha_m\dot{\mathbf{a}}_m\mathbf{v}_m^{\mathrm{T}}+\alpha_m\mathbf{a}_m\dot{\mathbf{v}}_m^{\mathrm{T}}\right)\mathbf{X}_m, \qquad (16)$$

$$\frac{d\boldsymbol{\mu}_{m,\mathrm{cbf}}}{d\alpha_m^{\mathrm{R}}}=\mathbf{a}_m\mathbf{v}_m^{\mathrm{T}}\mathbf{X}_m. \qquad (17)$$

We get (13)-(15) using (16) and (17) and the cyclic property of the trace operation: $\mathrm{tr}(ABC)=\mathrm{tr}(BCA)$ in (7). □

3) Coordinated Multipoint Enabling Bi-Static Sensing: In the case of CoMP, ICR becomes useful as an additional source of bi-static sensing, in addition to the serving BS's mono-static sensing. However, the ICR-related parameters $\{\{\theta_n\},\{\alpha_n\}\}\triangleq\{\boldsymbol{\theta}_n,\boldsymbol{\alpha}_n\}$ are unknown to the m^{th} Bs. The set of unknown parameters associated with BS m in the CoMP mode is represented as $\boldsymbol{\eta}_{m,\mathrm{comp}}=\{\boldsymbol{\theta}_n,\alpha_m^{\mathrm{R}},\alpha_m^{\mathrm{I}},\boldsymbol{\alpha}_n^{\mathrm{R}},\boldsymbol{\alpha}_n^{\mathrm{I}}\}$. The FIM for the CoMP case $\mathbf{F}_{m,\mathrm{comp}}$ is similar to (10) with the entries computed using Proposition 2.

Proposition 2. *For the m^{th} BS configured in CoMP mode, the FIM is expressed as*

$$\mathbf{F}_{m,\mathrm{comp}}=2\begin{bmatrix}F_{\theta_m\theta_m}^{\mathrm{R}} & \mathbf{f}_{\theta_m\boldsymbol{\eta}_{m,\mathrm{comp}}}\\ \mathbf{f}_{\theta_m\boldsymbol{\eta}_{m,\mathrm{comp}}}^{\mathrm{T}} & \mathbf{F}_{\boldsymbol{\eta}_{m,\mathrm{comp}}\boldsymbol{\eta}_{m,\mathrm{comp}}}\end{bmatrix}. \qquad (18)$$

The entries of the FIM are computed using using (19)-(26)*, where $\mathbf{D}_m=\mathrm{diag}(\mathbf{0}_{N_{\mathrm{tx}}},..,\mathbf{I}_{N_{\mathrm{tx}}},..,\mathbf{0}_{N_{\mathrm{tx}}})\in\mathcal{C}^{N\times N}$; $\mathbf{v}_m^{'}=\{\vec{0}_{N_{\mathrm{tx}}},..,\mathbf{v}_m,..,\vec{0}_{N_{\mathrm{tx}}}\}\in\mathcal{C}^{N\times 1}$, and $\hat{\mathbf{R}}_{\mathbf{X}_{op}}=\mathbf{D}_o\mathbf{R}_{\mathbf{X}}\mathbf{D}_p^{\mathrm{H}}\ \forall o,p\in\{m,n\}$.*

Proof. Since each BS knows the transmitted symbol matrix of the other BSs, the ICR of (5) aids the target's angle estimation in a bi-static manner. Consequently, the received echo at the m^{th} BS is a multi-variate Gaussian random variable with mean $\boldsymbol{\mu}_{m,\mathrm{cmp}}=\mathbf{G}_m^{'}\mathbf{D}_m\mathbf{X}+\sum_{n\neq m}^{J}\mathbf{G}_n^{'}\mathbf{D}_n\mathbf{X}$ where $\mathbf{G}_n^{'}=\alpha_n\mathbf{a}_m\mathbf{v}_n^{'\mathrm{T}}$ and the covariance matrix $\mathbf{C}_{m,\mathrm{cmp}}=\sigma_{\mathrm{R}}^2\mathbf{I}_{N_{\mathrm{rx}}}$. Hence,

$$\begin{aligned}\frac{d\boldsymbol{\mu}_{m,\mathrm{cmp}}}{d\theta_m} &= \alpha_m\underbrace{\left[\dot{\mathbf{a}}_m\mathbf{v}_m^{'\mathrm{T}}+\mathbf{a}_m\dot{\mathbf{v}}_m^{'\mathrm{T}}\right]}_{\dot{\mathbf{G}}_{m,\theta_m}}\mathbf{D}_m\mathbf{X}\\ &+\sum_{n\neq m}^{J}\alpha_n\underbrace{\dot{\mathbf{a}}_m\mathbf{v}_n^{'\mathrm{T}}}_{\dot{\mathbf{G}}_{n,\theta_m}}\mathbf{D}_n\mathbf{X}, \qquad (27)\\ \frac{d\boldsymbol{\mu}_{m,\mathrm{cmp}}}{d\theta_n} &= \alpha_n\underbrace{\mathbf{a}_m\dot{\mathbf{v}}_n^{'\mathrm{T}}}_{\dot{\mathbf{G}}_{n,\theta_n}}\mathbf{D}_n\mathbf{X}, \qquad (28)\\ \frac{d\boldsymbol{\mu}_{m,\mathrm{cmp}}}{d\alpha_o} &= \underbrace{\left[\mathbf{a}_m\mathbf{v}_o^{'\mathrm{T}}\right]}_{\dot{\mathbf{G}}_{o,\alpha_o}}\mathbf{D}_o\mathbf{X},\quad \forall o\in\{m,n\}. \qquad (29)\end{aligned}$$

Equations (19), (23)- (26) are obtained using (27) - (29) in (7). □

The corresponding Fisher Information matrices, $\mathbf{F}_{m,\mathrm{cbf}}$ and $\mathbf{F}_{m,\mathrm{comp}}$, are obtained using (13)-(15) and (19)- (21) in (10). The following problem formulations optimise the precoders towards a specific direction of interest [37].

III. Robust Block Level Precoding

The BLP constrains the co-channel interference experienced by a user so that the received symbol is within a certain distance from the nominal constellation symbol. In this section, we explain the BLP design framework for CBF and CoMP BS coordination schemes.

A. BLP: Coordinated Beamforming

We take a worst-case approach for the transmit precoding design to guarantee the resulting solution is robust to all possible channel uncertainties within $\mathcal{E}_{mk}$. Hence, in the CBF mode, for the m^{th} BS, we aim to solve the following optimization problem:

$$\begin{aligned}(\mathrm{P1}):\ &\underset{\{\mathbf{w}_{mk},t_{m,\mathrm{cbf}},\gamma\}}{\text{maximize}}\ \frac{\rho\cdot t_{m,\mathrm{cbf}}}{\mathrm{NF}_{\mathrm{R,cbf}}^{\mathrm{blp}}}+\frac{(1-\rho)\cdot\gamma}{\mathrm{NF}_{\mathrm{C,cbf}}^{\mathrm{blp}}},\\ &\text{s.t.}\begin{bmatrix}F_{\theta_m\theta_m}^{\mathrm{R}}-t_{m,\mathrm{cbf}} & \mathbf{f}_{\theta_m\boldsymbol{\eta}_{m,\mathrm{cbf}}}\\ \mathbf{f}_{\theta_m\boldsymbol{\eta}_{m,\mathrm{cbf}}}^{\mathrm{T}} & \mathbf{F}_{\boldsymbol{\eta}_{m,\mathrm{cbf}}\boldsymbol{\eta}_{m,\mathrm{cbf}}}\end{bmatrix}\succeq\mathbf{0}, \qquad (30a)\\ &\min_{\mathbf{e}_{mk}}\left(\gamma_{mk}\right)\geq\gamma\quad\forall U_{mk}, \qquad (30b)\\ &\sum_{k=1}^{K}\mathrm{tr}\left(\mathbf{w}_{mk}\mathbf{w}_{mk}^{\mathrm{H}}\right)\leq P_{\mathrm{t}}, \qquad (30c)\end{aligned}$$

where

$$\gamma_{mk}=\frac{|\tilde{\mathbf{h}}_{m,mk}^{\mathrm{T}}\mathbf{w}_{mk}|^2}{\underbrace{\sum_{l\neq k}^{K}|\tilde{\mathbf{h}}_{m,mk}^{\mathrm{T}}\mathbf{w}_{ml}|^2}_{\mathrm{InCI}_{mk}}+\sum_{n\neq m}^{J}\underbrace{\sum_{l=1}^{K}|\tilde{\mathbf{h}}_{n,mk}^{\mathrm{T}}\mathbf{w}_{nl}|^2}_{\mathrm{ICI}_{n,mk}}+\sigma_{\mathrm{C}}^2}, \qquad (31)$$

is the received SINR at U_{mk} obtained using (2). The objective function of (P1) is the weighted sum of two components: minimizing the CRB in estimating the target's angle and

This article has been accepted for publication in IEEE Transactions on Wireless Communications. This is the author's version which has not been fully edited and content may change prior to final publication. Citation information: DOI 10.1109/TWC.2024.3417713

$$F_{\theta_m\theta_m} = \mathrm{tr}\Bigg(|\alpha_m|^2\dot{\mathbf{G}}_{m,\theta_m}\hat{\mathbf{R}}_{\mathbf{X}_{mm}}\dot{\mathbf{G}}^{\mathrm{H}}_{m,\theta_m} + \sum_{n\neq m}^{J}\alpha_n^*\alpha_m\dot{\mathbf{G}}_{m,\theta_m}\hat{\mathbf{R}}_{\mathbf{X}_{mn}}\dot{\mathbf{G}}^{\mathrm{H}}_{n,\theta_m} + \alpha_m^*\alpha_n\dot{\mathbf{G}}_{n,\theta_m}\hat{\mathbf{R}}_{\mathbf{X}_{nm}}\dot{\mathbf{G}}^{\mathrm{H}}_{m,\theta_m} + \sum_{n\neq m}^{J}\sum_{n\neq m}^{J}|\alpha_n|^2\dot{\mathbf{G}}_{n,\theta_m}\hat{\mathbf{R}}_{\mathbf{X}_{nn}}\dot{\mathbf{G}}^{\mathrm{H}}_{n,\theta_m}\Bigg) \quad \mathcal{C}^{1\times 1} \tag{19}$$

$$\mathbf{f}_{\theta_m\boldsymbol{\eta}_{m,\mathrm{comp}}} = \frac{L}{\sigma_{\mathrm{R}}^2}[\mathbf{f}^{\mathrm{R}}_{\theta_m\boldsymbol{\theta}_n}, F^{\mathrm{R}}_{\theta_m\alpha_m}, -F^{\mathrm{I}}_{\theta_m\alpha_m}, \mathbf{f}^{\mathrm{R}}_{\theta_m\boldsymbol{\alpha}_n}, -\mathbf{f}^{\mathrm{I}}_{\theta_m\boldsymbol{\alpha}_n}] \quad \in \mathcal{C}^{1\times(3\cdot J-1)} \tag{20}$$

$$\mathbf{F}_{\boldsymbol{\eta}_{m,\mathrm{comp}}\boldsymbol{\eta}_{m,\mathrm{comp}}} = \frac{L}{\sigma_{\mathrm{R}}^2}\begin{bmatrix} \mathbf{F}^{\mathrm{R}}_{\boldsymbol{\theta}_n\boldsymbol{\theta}_n} & \mathbf{f}^{\mathrm{R}}_{\boldsymbol{\theta}_n\alpha_m} & -\mathbf{f}^{\mathrm{I}}_{\boldsymbol{\theta}_n\alpha_m} & \mathbf{F}^{\mathrm{R}}_{\boldsymbol{\theta}_n\boldsymbol{\alpha}_n} & -\mathbf{F}^{\mathrm{I}}_{\boldsymbol{\theta}_n\boldsymbol{\alpha}_n} \\ \mathbf{f}^{\mathrm{R}^{\mathrm{T}}}_{\boldsymbol{\theta}_n\alpha_m} & F^{\mathrm{R}}_{\alpha_m\alpha_m} & -F^{\mathrm{I}}_{\alpha_m\alpha_m} & \mathbf{f}^{\mathrm{R}}_{\alpha_m\boldsymbol{\alpha}_n} & -\mathbf{f}^{\mathrm{I}}_{\alpha_m\boldsymbol{\alpha}_n} \\ -\mathbf{f}^{\mathrm{I}^{\mathrm{T}}}_{\boldsymbol{\theta}_n\alpha_m} & -F^{\mathrm{I}}_{\alpha_m\alpha_m} & F^{\mathrm{R}}_{\alpha_m\alpha_m} & -\mathbf{f}^{\mathrm{I}}_{\alpha_m\boldsymbol{\alpha}_n} & \mathbf{f}^{\mathrm{R}}_{\alpha_m\boldsymbol{\alpha}_n} \\ \mathbf{F}^{\mathrm{R}^{\mathrm{T}}}_{\boldsymbol{\theta}_n\boldsymbol{\alpha}_n} & \mathbf{f}^{\mathrm{R}^{\mathrm{T}}}_{\alpha_m\boldsymbol{\alpha}_n} & -\mathbf{f}^{\mathrm{I}^{\mathrm{T}}}_{\alpha_m\boldsymbol{\alpha}_n} & \mathbf{F}^{\mathrm{R}}_{\boldsymbol{\alpha}_n\boldsymbol{\alpha}_n} & -\mathbf{F}^{\mathrm{I}}_{\boldsymbol{\alpha}_n\boldsymbol{\alpha}_n} \\ -\mathbf{F}^{\mathrm{I}^{\mathrm{T}}}_{\boldsymbol{\theta}_n\boldsymbol{\alpha}_n} & -\mathbf{f}^{\mathrm{I}^{\mathrm{T}}}_{\alpha_m\alpha_n} & \mathbf{f}^{\mathrm{R}^{\mathrm{T}}}_{\alpha_m\boldsymbol{\alpha}_n} & -\mathbf{F}^{\mathrm{I}^{\mathrm{T}}}_{\boldsymbol{\alpha}_n\boldsymbol{\alpha}_n} & \mathbf{F}^{\mathrm{R}^{\mathrm{T}}}_{\boldsymbol{\alpha}_n\boldsymbol{\alpha}_n} \end{bmatrix}, \quad \in \mathcal{C}^{(3\cdot J-1)\times(3\cdot J-1)} \tag{21}$$

$\mathbf{f}_{\theta_m\boldsymbol{\theta}_n} = [F_{\theta_m\theta_n}] \in \mathcal{C}^{1\times(J-1)}; F_{\theta_m\alpha_m} \in \mathcal{C}^{1\times 1}; \mathbf{f}_{\theta_m\boldsymbol{\alpha}_n} = [F_{\theta_m\alpha_n}] \in \mathcal{C}^{1\times(J-1)}; \mathbf{F}_{\boldsymbol{\theta}_n\boldsymbol{\theta}_n} = [F_{\theta_n\theta_n}] \in \mathcal{C}^{(J-1)\times(J-1)}; F_{\alpha_m\alpha_m} \in \mathcal{C}^{1\times 1};$
$\mathbf{f}_{\boldsymbol{\theta}_n\alpha_m} = [F_{\theta_n\alpha_m}] \in \mathcal{C}^{(J-1)\times 1}; \mathbf{F}_{\boldsymbol{\theta}_n\boldsymbol{\alpha}_n} = [F_{\theta_n\alpha_n}] \in \mathcal{C}^{(J-1)\times(J-1)}; \mathbf{F}_{\boldsymbol{\alpha}_n\boldsymbol{\alpha}_n} = [F_{\alpha_n\alpha_n}] \in \mathcal{C}^{(J-1)\times(J-1)};$
$\mathbf{f}_{\alpha_m\boldsymbol{\alpha}_n} = [F_{\alpha_m\alpha_n}] \in \mathcal{C}^{1\times(J-1)};$ (22)

$$F_{\theta_m\theta_n} = \mathrm{tr}\left(\alpha_m^*\alpha_n\dot{\mathbf{G}}_{n,\theta_n}\hat{\mathbf{R}}_{\mathbf{X}_{nm}}\dot{\mathbf{G}}^{\mathrm{H}}_{m,\theta_m} + |\alpha_n|^2\dot{\mathbf{G}}_{n,\theta_n}\hat{\mathbf{R}}_{\mathbf{X}_{nn}}\dot{\mathbf{G}}^{\mathrm{H}}_{n,\theta_m}\right); \quad F_{\theta_n\theta_n} = \mathrm{tr}\left(|\alpha_n|^2\dot{\mathbf{G}}_{n,\theta_n}\hat{\mathbf{R}}_{\mathbf{X}_{nn}}\dot{\mathbf{G}}^{\mathrm{H}}_{n,\theta_n}\right); \tag{23}$$

$$F_{\theta_m\alpha_m} = \mathrm{tr}\left(\alpha_m^*\dot{\mathbf{G}}_{m,\alpha_m}\hat{\mathbf{R}}_{\mathbf{X}_{mm}}\dot{\mathbf{G}}^{\mathrm{H}}_{m,\theta_m} + \alpha_n^*\dot{\mathbf{G}}_{m,\alpha_m}\hat{\mathbf{R}}_{\mathbf{X}_{mn}}\dot{\mathbf{G}}^{\mathrm{H}}_{n,\theta_m}\right); \quad F_{\theta_n\alpha_m} = \mathrm{tr}\left(\alpha_n^*\dot{\mathbf{G}}_{m,\alpha_m}\hat{\mathbf{R}}_{\mathbf{X}_{mn}}\dot{\mathbf{G}}^{\mathrm{H}}_{n,\theta_n}\right); \tag{24}$$

$$F_{\theta_m\alpha_n} = \mathrm{tr}\left(\alpha_m^*\dot{\mathbf{G}}_{n,\alpha_n}\hat{\mathbf{R}}_{\mathbf{X}_{nm}}\dot{\mathbf{G}}^{\mathrm{H}}_{m,\theta_m} + \alpha_n^*\dot{\mathbf{G}}_{n,\alpha_n}\hat{\mathbf{R}}_{\mathbf{X}_{nn}}\dot{\mathbf{G}}^{\mathrm{H}}_{n,\theta_m}\right); \quad F_{\theta_n\alpha_n} = \mathrm{tr}\left(\alpha_n^*\dot{\mathbf{G}}_{n,\alpha_n}\hat{\mathbf{R}}_{\mathbf{X}_{nn}}\dot{\mathbf{G}}^{\mathrm{H}}_{n,\theta_n}\right); \tag{25}$$

$$F_{\alpha_m\alpha_m} = \mathrm{tr}\left(\dot{\mathbf{G}}_{m,\alpha_m}\hat{\mathbf{R}}_{\mathbf{X}_{mm}}\dot{\mathbf{G}}^{\mathrm{H}}_{m,\alpha_m}\right); \quad F_{\alpha_m\alpha_n} = \mathrm{tr}\left(\dot{\mathbf{G}}_{n,\alpha_n}\hat{\mathbf{R}}_{\mathbf{X}_{nm}}\dot{\mathbf{G}}^{\mathrm{H}}_{m,\alpha_m}\right); \quad F_{\alpha_n\alpha_n} = \mathrm{tr}\left(\dot{\mathbf{G}}_{n,\alpha_n}\hat{\mathbf{R}}_{\mathbf{X}_{nn}}\dot{\mathbf{G}}^{\mathrm{H}}_{n,\alpha_n}\right). \tag{26}$$

maximizing the minimum SINR value among the users of the m^{th} cell. The weighting factor, $\rho \in [0,1]$, determines the balance between the communication and sensing performance matrices. The normalization factors $\mathrm{NF}^{\mathrm{blp}}_{\mathrm{R,cbf}}$ and $\mathrm{NF}^{\mathrm{blp}}_{\mathrm{C,cbf}}$ are determined by solving (P1) for $\rho = 1$ and $\rho = 0$, respectively. Using (30a), we limit Fisher information value to be less than or equal to $t_{m,\mathrm{cbf}}$ using the Schur complement: $F^{\mathrm{R}}_{\theta_m\theta_m} - \mathbf{f}_{\theta_m\boldsymbol{\eta}_{m,\mathrm{cbf}}}\mathbf{F}_{\boldsymbol{\eta}_{m,\mathrm{cbf}}\boldsymbol{\eta}_{m,\mathrm{cbf}}}\mathbf{f}^{\mathrm{T}}_{\theta_m\boldsymbol{\eta}_{m,\mathrm{cbf}}} >= t_{m.\mathrm{cbf}}$. Moreover, (30b) is the SINR constraint derived from (2), whereas (30c) is the total power constraint with P_{t} being the total available power at the BS. Problem (P1) is difficult to solve because of (a) the infinite possibilities of $\mathbf{e}_{mk}$ in (30b), (b) the non-convex multiplication between γ and the interference terms in (30b) and (c) the non-convex form of $\mathbf{C}_{m,\mathrm{cbf}}$ in (30a).

We tackle the infinite possibilities of $\mathbf{e}_{mk}$ by representing it as the ratio of the minimum of the numerator to the maximum of the denominator:

$$\frac{\min\limits_{\mathbf{e}_{mk}}(|\tilde{\mathbf{h}}^{\mathrm{T}}_{m,mk}\mathbf{w}_{mk}|^2)}{\max\limits_{\mathbf{e}_{mk}}(\mathrm{InCI}_{mk} + \sum_{n\neq m}^{J}\mathrm{ICI}_{n,mk} + \sigma_{\mathrm{C}}^2)} \geq \gamma. \tag{32}$$

The minimum value of the numerator and the maximum value of the denominator of (32) can be determined using Proposition 3.

Proposition 3. *For a given CSI uncertainty set $\mathcal{E}_{mk} = \{\mathbf{e}_{mk} : \|\mathbf{e}_{mk}\|^2 \leq \delta^2\}$, the following equalities hold for any U_{mk}.*

$$\min_{\mathbf{e}_{mk}}|\tilde{\mathbf{h}}^{\mathrm{T}}_{m,mk}\mathbf{w}_{mk}|^2 = \mathrm{tr}\left(\mathbf{Q}_{m,mk}\mathbf{W}_{mk}\right), \tag{33}$$

$$\max_{\mathbf{e}_{mk}}\left(|\tilde{\mathbf{h}}^{\mathrm{T}}_{m,mk}\mathbf{w}_{mk}|^2\right) = \mathrm{tr}\left(\mathbf{Q}_{m,mk}\mathbf{W}_{mk}\right) + \delta^2\mathrm{tr}\left(\mathbf{W}_{mk}\right) + \delta\|\mathbf{h}^{\mathrm{T}}_{m,mk}\mathbf{W}_{mk}\| + \delta\|\mathbf{W}_{mk}\mathbf{h}^*_{m,mk}\|, \tag{34}$$

where $\mathbf{Q}_{m,mk} = \mathbf{h}^*_{m,mk}\mathbf{h}^{\mathrm{T}}_{m,mk}$ and $\mathbf{W}_{mk} = \mathbf{w}_{mk}\mathbf{w}^{\mathrm{H}}_{mk}$.

Proof. Let,

$$|\tilde{\mathbf{h}}^{\mathrm{T}}_{m,mk}\mathbf{w}_{mk}|^2 = \mathrm{tr}\left(\tilde{\mathbf{Q}}_{m,mk}\mathbf{W}_{mk}\right) \tag{35}$$
$$= \mathrm{tr}\left(\tilde{\mathbf{h}}^*_{m,mk}\tilde{\mathbf{h}}^{\mathrm{T}}_{m,mk}\mathbf{W}_{mk}\right) \tag{36}$$
$$= \mathrm{tr}\left(\tilde{\mathbf{h}}^{\mathrm{T}}_{m,mk}\mathbf{W}_{mk}\tilde{\mathbf{h}}^*_{m,mk}\right) \tag{37}$$
$$= \mathrm{tr}\left(\left(\mathbf{h}^{\mathrm{T}}_{m,mk} + \mathbf{e}^{\mathrm{T}}_{mk}\right)\mathbf{W}_{mk}\left(\mathbf{h}^*_{m,mk} + \mathbf{e}^*_{mk}\right)\right) \tag{38}$$
$$= \mathrm{tr}\left(\mathbf{h}^{\mathrm{T}}_{m,mk}\mathbf{W}_{mk}\mathbf{h}^*_{m,mk}\right) + \mathrm{tr}\left(\mathbf{h}^{\mathrm{T}}_{m,mk}\mathbf{W}_{mk}\mathbf{e}^*_{mk}\right) + \mathrm{tr}\left(\mathbf{e}^{\mathrm{T}}_{mk}\mathbf{W}_{mk}\mathbf{h}^*_{m,mk}\right) + \mathrm{tr}\left(\mathbf{e}^{\mathrm{T}}_{mk}\mathbf{W}_{mk}\mathbf{e}^*_{mk}\right). \tag{39}$$

Now,

$$\max_{\|\mathbf{e}_{mk}\|^2\leq\delta^2}\mathrm{tr}\left(\tilde{\mathbf{Q}}_{m,mk}\mathbf{W}_{mk}\right) = \mathrm{tr}\left(\mathbf{Q}_{m,mk}\mathbf{W}_{mk}\right) + \|\mathbf{h}^{\mathrm{T}}_{m,mk}\mathbf{W}_{mk}\mathbf{e}^*_{mk}\| + \|\mathbf{e}^{\mathrm{T}}_{mk}\mathbf{W}_{mk}\mathbf{h}^*_{m,mk}\| + \mathrm{tr}\left(\mathbf{e}^*_{mk}\mathbf{e}^{\mathrm{T}}_{mk}\mathbf{W}_{mk}\right) \tag{40}$$

$$\leq \mathrm{tr}\left(\mathbf{Q}_{m,mk}\mathbf{W}_{mk}\right) + \delta\|\mathbf{h}^{\mathrm{T}}_{m,mk}\mathbf{W}_{mk}\| + \delta\|\mathbf{W}_{mk}\mathbf{h}^*_{m,mk}\| + \mathrm{tr}\left(\mathbf{e}^*_{mk}\mathbf{e}^{\mathrm{T}}_{mk}\right)\mathrm{tr}\left(\mathbf{W}_{mk}\right)$$
$$\leq \mathrm{tr}\left(\mathbf{Q}_{m,mk}\mathbf{W}_{mk}\right) + \delta\|\mathbf{h}^{\mathrm{T}}_{m,mk}\mathbf{W}_{mk}\| + \delta\|\mathbf{W}_{mk}\mathbf{h}^*_{m,mk}\| + \delta^2\mathrm{tr}\left(\mathbf{W}_{mk}\right). \tag{41}$$

Here, (41) is derived from (40) using Cauchy-Schwarz inequality. The minimum value of the numerator is obtained by substituting $\delta = 0$ in (41). □

This article has been accepted for publication in IEEE Transactions on Wireless Communications. This is the author's version which has not been fully edited and content may change prior to final publication. Citation information: DOI 10.1109/TWC.2024.3417713

Consequently,

$$\max_{\mathbf{e}_{mk}}(\mathrm{InCI}_{mk}) = \sum_{l\neq k}^{K} \mathrm{tr}\left(\mathbf{Q}_{m,mk}\mathbf{W}_{ml}\right) + \delta\|\mathbf{h}_{m,mk}^{\mathrm{T}}\mathbf{W}_{ml}\| + \delta\|\mathbf{W}_{ml}\mathbf{h}_{m,mk}^{*}\| + \delta^2\mathrm{tr}\left(\mathbf{W}_{ml}\right), \quad (42)$$

$$\max_{\mathbf{e}_{mk}}(\mathrm{ICI}_{n,mk}) = \sum_{l=1}^{K} \mathrm{tr}\left(\mathbf{Q}_{n,mk}\mathbf{W}_{nl}\right) + \delta\|\mathbf{h}_{n,mk}^{\mathrm{T}}\mathbf{W}_{nl}\| + \delta\|\mathbf{W}_{nl}\mathbf{h}_{n,mk}^{*}\| + \delta^2\mathrm{tr}\left(\mathbf{W}_{nl}\right). \quad (43)$$

The non-convex multiplication between γ and the interference terms in (30b) is addressed by representing (30b) through a set of intra-cell and inter-cell leakage constraints (44)-(46):

$$\max_{\mathbf{e}_{mk}}(\mathrm{InCI}_{mk}) \leq I_{m,\mathrm{cbf}}^{\mathrm{intra}},\ \forall U_{mk}, \quad (44)$$

$$\max_{\mathbf{e}_{nk}}(\mathrm{ICI}_{m,nk}) \leq \frac{I_{\mathrm{cbf}}^{\mathrm{inter}}}{J-1}\ \forall U_{nk}\, n\neq m, \quad (45)$$

$$\mathrm{tr}\left(\mathbf{Q}_{m,mk}\mathbf{W}_{mk}\right) - \gamma(I_{m,\mathrm{cbf}}^{\mathrm{intra}} + I_{\mathrm{cbf}}^{\mathrm{inter}}) \geq \gamma\sigma_{\mathrm{C}}^2\ \forall U_{mk}. \quad (46)$$

Equation (44) limits the intracell interference to any user served by m^{th} BS to be less than $I_{m,\mathrm{cbf}}^{\mathrm{intra}}$. The left-hand-side (LHS) of (45) gives the maximum ICI from m^{th} BS to U_{nk}. The constraint (45) satisfied by all the BSs restricts the ICI to any user in the system to $I_{\mathrm{cbf}}^{\mathrm{inter}}$. Note that for given $I_{m,\mathrm{cbf}}^{\mathrm{intra}}$ and $I_{\mathrm{cbf}}^{\mathrm{inter}}$ values, the constraints (44)-(46) become convex. Lastly, for a given $\{\mathbf{W}_{nk}\}$, $\mathbf{C}_{m,\mathrm{cbf}}$ can be estimated using (9), which makes the entries of $\mathbf{F}_{m,\mathrm{cbf}}$ of (30a), an affine function function of $\mathbf{R}_{\mathbf{X}_m} = \sum_k^K \mathbf{W}_{mk}$. Hence, we solve (P1) by solving the following two optimization problems alternatively:

$$(\mathrm{P1.A}): \underset{\{\mathbf{W}_{mk}, t_{m,\mathrm{cbf}}, \gamma\}}{\text{maximize}} \quad \frac{\rho\cdot t_{m,\mathrm{cbf}}}{\mathrm{NF}_{\mathrm{R,cbf}}^{\mathrm{blp}}} + \frac{(1-\rho)\cdot\gamma}{\mathrm{NF}_{\mathrm{C,cbf}}^{\mathrm{blp}}},$$

$$\text{s.t.} \sum_{k=1}^{K} \mathrm{tr}\left(\mathbf{W}_{mk}\right) \leq P_{\mathrm{t}}, \quad (47a)$$

$$\mathrm{rank}(\mathbf{W}_{mk}) = 1;\ \mathbf{W}_{mk}\succeq\mathbf{0}, \quad (47b)$$

$$(30a), (44) - (46). \quad (47c)$$

$$(\mathrm{P1.B}): \underset{\{\mathbf{W}_{mk}, I_{m,\mathrm{cbf}}^{\mathrm{intra}}, I_{m,\mathrm{cbf}}^{\mathrm{inter}}\}}{\text{minimize}} \quad \frac{I_{m,\mathrm{cbf}}^{\mathrm{intra}}}{I_{\max}^{\mathrm{intra}}} + \frac{I_{m,\mathrm{cbf}}^{\mathrm{inter}}}{(J-1)\cdot I_{\max}^{\mathrm{inter}}},$$

$$\text{s.t.} \begin{bmatrix} F_{\theta_m\theta_m}^{\mathrm{R}} - t_{m,\mathrm{cbf}}^{*} & \mathbf{f}_{\theta_m\boldsymbol{\eta}_{m,\mathrm{cbf}}} \\ \mathbf{f}_{\theta_m\boldsymbol{\eta}_{m,\mathrm{cbf}}}^{\mathrm{T}} & \mathbf{F}_{\boldsymbol{\eta}_{m,\mathrm{cbf}}\boldsymbol{\eta}_{m,\mathrm{cbf}}} \end{bmatrix} \succeq \mathbf{0}, \quad (48a)$$

$$\mathrm{tr}\left(\mathbf{Q}_{m,mk}\mathbf{W}_{mk}\right) - \gamma^{*}\left(I_{m,\mathrm{cbf}}^{\mathrm{intra}} + I_{\mathrm{cbf}}^{\mathrm{inter}}\right) \geq \gamma^{*}\sigma_R^2, \quad (48b)$$

$$\max_{\mathbf{e}_{nk}}(\mathrm{ICI}_{m,nk}) \leq \frac{I_{m,\mathrm{cbf}}^{\mathrm{inter}}}{J-1};\ I_{m,\mathrm{cbf}}^{\mathrm{inter}} \leq I_{\mathrm{cbf}}^{\mathrm{inter}}, \quad (48c)$$

$$(47a), (44), (47b). \quad (48d)$$

The first problem, (P1.A), minimizes the CRB and maximizes the minimum communication SINR for a given $\{\mathbf{W}_{nk}\}$ $\forall n \neq m \in \mathcal{J}$, $I_{m,\mathrm{cbf}}^{\mathrm{intra}}$, and $I_{\mathrm{cbf}}^{\mathrm{inter}}$ values. Equation (47a) is the equivalent representation of (30c). Using the solution of (P1.A): γ^{*}, and $\mathrm{t}_{m,\mathrm{cbf}}^{*}$, (P1.B) minimizes the leakage power towards the neighbouring BSs' users while guaranteeing given sensing and communication performance through (48a) and (48b). Here, $I_{\max}^{\mathrm{intra}}$ and $I_{\max}^{\mathrm{intra}}$ represent the maximum tolerable intra-cell and inter-cell interference values, respectively. Omitting the rank constraint, (P1.A) and (P1.B) are convex optimization problems solved using MATLAB's CVX solver [38]. The overall procedure is given in Algorithm 1. In the CBF mode, initially, all BSs select beamforming vectors $\mathbf{w}_{mk}$ randomly and estimate their covariance matrices $\mathbf{C}_{m,\mathrm{cbf}}$. Each BS then independently solves (P1.A) to optimize the weighted combination of sensing and communication performance in parallel. Subsequently, (P1.B) is solved to minimize interference to neighbouring BSs, using the solutions from (P1.A). A similar approach is used in the CoMP mode, as outlined in steps 7-9. We can obtain $\mathbf{w}_{mk}$ from $\mathbf{W}_{mk}$ using Eigenvalue decomposition technique if the rank of $\mathbf{W}_{mk} > 1$ [17].

B. BLP: Coordinated Multi-point

The corresponding optimization problem in the CoMP scenario can be formulated as,

$$(\mathrm{P2}): \underset{\{\mathbf{W}_k f, \gamma\}}{\text{maximize}} \quad \frac{f\cdot\rho}{\mathrm{NF}_{\mathrm{R,comp}}^{\mathrm{blp}}} + \frac{(1-\rho)\cdot\gamma}{\mathrm{NF}_{\mathrm{C,comp}}^{\mathrm{blp}}},$$

$$\text{s.t.} \begin{bmatrix} F_{\theta_m\theta_m}^{\mathrm{R}} - t_{m,\mathrm{comp}} & \mathbf{f}_{\theta_m\boldsymbol{\eta}_{m,\mathrm{comp}}} \\ \mathbf{f}_{\theta_m\boldsymbol{\eta}_{m,\mathrm{comp}}}^{\mathrm{T}} & \mathbf{F}_{\boldsymbol{\eta}_{m,\mathrm{comp}}\boldsymbol{\eta}_{m,\mathrm{comp}}} \end{bmatrix} \succeq \mathbf{0}, \quad (49a)$$

$$t_{m,\mathrm{comp}} \geq f, \quad \forall m, \quad (49b)$$

$$\min_{\mathbf{e}_k} \underbrace{\left(\frac{|\tilde{\mathbf{h}}_k^{\mathrm{T}}\mathbf{w}_k|^2}{\sum_{l\neq k}^{JK}|\tilde{\mathbf{h}}_k^{\mathrm{T}}\mathbf{w}_l|^2 + \sigma_{\mathrm{C}}^2}\right)}_{\gamma_k} \geq \gamma,\ \forall k, \quad (49c)$$

$$\sum_{k=1}^{K} \mathrm{tr}\left(\mathbf{D}_m\mathbf{w}_k\mathbf{w}_k^{\mathrm{H}}\mathbf{D}_m^{\mathrm{H}}\right) \leq P_{\mathrm{t}}, \forall m. \quad (49d)$$

The objective function of (P2) is the weighted combination of minimizing the maximum CRB and maximizing the minimum SINR values. Using (49a), we limit the Fisher information value to be less than or equal to $t_{m,\mathrm{comp}}$ using the Schur complement:$F_{\theta_m\theta_m}^{\mathrm{R}} - \mathbf{f}_{\theta_m\boldsymbol{\eta}_{m,\mathrm{comp}}}^{\mathrm{T}}\mathbf{F}_{\boldsymbol{\eta}_{m,\mathrm{comp}}\boldsymbol{\eta}_{m,\mathrm{comp}}}\mathbf{f}_{\theta_m\boldsymbol{\eta}_{m,\mathrm{comp}}} >= t_{m,\mathrm{comp}}$. In (49b), f is defined as the minimum Fisher information value for estimating θ_m. Equation (49c) is the minimum SINR constraint written using (4) whereas (49d) is the per-BS power constraint. The constants $\mathrm{NF}_{\mathrm{R,comp}}^{\mathrm{blp}}$ and $\mathrm{NF}_{\mathrm{C,comp}}^{\mathrm{blp}}$ are the corresponding maximum values of f and γ obtained by setting $\rho = 1$ and $\rho = 0$, respectively. Here, $\mathbf{w_k} = [\mathbf{w}_{1k}; \mathbf{w}_{2k;\ldots;}\mathbf{w}_{Jk}]\,\mathcal{C}^{N\times 1}$ represents the precoding vectors for user k from all the BSs stacked vertically. Problem (P2) is non-convex due to the infinite possibilities of $\mathbf{e}_k$ and the non-convex SINR constraint (49c). Similar to the CBF case, we tackle the infinite possibilities of $\mathbf{e}_k$ by adapting Proposition 3 to the CoMP case. Using Proposition 3, we have

$$\min_{\mathbf{e}_k}|\tilde{\mathbf{h}}_k^{\mathrm{T}}\mathbf{w}_k|^2 = \mathrm{tr}\left(\mathbf{Q}_k\mathbf{W}_k\right), \quad (50)$$

$$\max_{\mathbf{e}_k}\left(|\tilde{\mathbf{h}}_k^{\mathrm{T}}\mathbf{w}_l|^2\right) = \mathrm{tr}\left(\mathbf{Q}_k\mathbf{W}_l\right) + J\delta^2\mathrm{tr}\left(\mathbf{W}_l\right) + \sqrt{J}\delta\|\mathbf{h}_k^{\mathrm{T}}\mathbf{W}_l\| + \sqrt{J}\delta\|\mathbf{W}_l\mathbf{h}_k^{*}\|, \quad (51)$$

This article has been accepted for publication in IEEE Transactions on Wireless Communications. This is the author's version which has not been fully edited and content may change prior to final publication. Citation information: DOI 10.1109/TWC.2024.3417713

where $\mathbf{Q}_k = \mathbf{h}_k\mathbf{h}_k^{\mathrm{H}} \in \mathcal{C}^{N\times N}$, $\mathbf{W}_k = \mathbf{w}_k\mathbf{w}_k^{\mathrm{H}} \in \mathcal{C}^{N\times N}$, and $\mathbf{R}_{\mathbf{X}} = \sum_{k=1}^{2K}\mathbf{W}_k$. Then, (49c) is reformulated into the following pair of constraints.

$$\mathrm{tr}\left(\mathbf{Q}_k\mathbf{W}_k\right) - \gamma I_{\mathrm{comp}} \geq \gamma\sigma_{\mathrm{C}}^2, \tag{52}$$

$$\sum_{l\neq k}^{JK} \max_{\mathbf{e}_k}\left(|\tilde{\mathbf{h}}_k^{\mathrm{T}}\mathbf{w}_l|^2\right) \leq I_{\mathrm{comp}}. \tag{53}$$

Equation (53) limits the total interference experienced by any user to be less than I_{comp}. For a given I_{comp} value, (52) and (53) become convex constraints. Hence, we solve (P2) by solving the (P2.A) and (P2.B) alternately.

$$(\mathrm{P2.A}): \underset{\{\mathbf{W}_k, f, \gamma\}}{\text{maximize}} \quad \frac{f\cdot\rho}{\mathrm{NF}_{\mathrm{R,comp}}^{\mathrm{blp}}} + \frac{(1-\rho)\cdot\gamma}{\mathrm{NF}_{\mathrm{C,comp}}^{\mathrm{blp}}},$$

$$\text{s.t.} \sum_{k=1}^{K}\mathrm{tr}\left(\mathbf{D}_m\mathbf{W}_k\mathbf{D}_m^{\mathrm{H}}\right) \leq P_{\mathrm{t}}, \tag{54a}$$

$$\mathbf{W}_k \succeq \mathbf{0}\ \forall k,\ \mathrm{rank}(\mathbf{W}_k) = 1, \tag{54b}$$

$$(49a), (49b), (52), (53). \tag{54c}$$

$$(\mathrm{P2.B}): \underset{\{\mathbf{W}_k, I_{\mathrm{comp}}\}}{\text{minimize}} \quad I_{\mathrm{comp}},$$

$$\text{s.t.} \begin{bmatrix} F_{\theta_m\theta_m}^{\mathrm{R}} - t_{m,\mathrm{comp}}^{*} & \mathbf{f}_{\theta_m\boldsymbol{\eta}_{m,\mathrm{comp}}} \\ \mathbf{f}_{\theta_m\boldsymbol{\eta}_{m,\mathrm{comp}}}^{\mathrm{T}} & \mathbf{F}_{\boldsymbol{\eta}_{m,\mathrm{comp}}\boldsymbol{\eta}_{m,\mathrm{comp}}} \end{bmatrix} \succeq \mathbf{0}, \tag{55a}$$

$$t_{m,\mathrm{comp}} \geq f^*, \quad \forall m, \tag{55b}$$

$$\mathrm{tr}\left(\mathbf{Q}_k\mathbf{W}_k\right) - \gamma^* I_{\mathrm{comp}} \geq \gamma\sigma_{\mathrm{C}}^2\ \forall k, \tag{55c}$$

$$(53), (54a), (54b). \tag{55d}$$

Problem (P2.A) maximizes the objective function of (P2) for a given maximum value of the co-channel interference I_{comp}. Equation (54a) is the equivalent representation of (49d). Problem (P2.B) minimizes the co-channel interference while guaranteeing a maximum CRB f^* and minimum SINR γ^* through (55a)-(55c). Dropping the rank constraints, (P2.A) and (P2.B) are convex optimization problems. Algorithm 1 summarizes the robust block-level precoder design procedure.

Algorithm 1: Robust Block Level Precoder Design

Input: u, $\{\mathbf{h}_{m,nk}\}$, $\{\mathbf{h}_k\}$, $I_{m,\mathrm{cbf}}^{\mathrm{intra}}$, $I_{\mathrm{cbf}}^{\mathrm{inter}}$,$\{\mathbf{W}_{mk}\}$, I_{comp};
while *no convergence* **do**
  if *BSs in CBF mode* **then**
    Determine $\mathbf{C}_{m,\mathrm{cbf}}$ using $\{\mathbf{W}_{mk}\}$ in (9);
    Solve (P1.A) for each BS to obtain γ^* and $\{t_{m,\mathrm{cbf}}^{*l}\}$;
    Solve (P1.B) to update $I_{m,\mathrm{cbf}}^{\mathrm{intra}}$, $I_{\mathrm{cbf}}^{\mathrm{inter}}$, $\{\mathbf{W}_{mk}\}$: $I_{\mathrm{cbf}}^{\mathrm{inter}} = \max\left(\{I_{m,\mathrm{cbf}}^{\mathrm{inter}}\}\right)$
  if *BSs in CoMP mode* **then**
    Solve (P2.A) to obtain γ^* and f^*;
    Solve (P2.B) to update I_{comp}: $I_{\mathrm{comp}} = \max\left(\{I_{m,\mathrm{comp}}\}\right)$
Output:$\{\mathbf{W}_{m,k}\}$, $\{\mathbf{W}_k\}$.

Note that, for a given γ, $\rho = 1$, $\delta = 0$ $J = 1$ setting, (P1), and (P2) are equivalent to the BLP design formulation, Eq. (18), of [11]. We verify the equivalence of the corresponding CRB expressions in Fig. 3. Certainly, our investigation into the multi-cell version of the CRB minimization problem introduces substantial differences in modeling. These distinctions make it impractical to directly apply the solutions presented in [11]. Furthermore, when $\delta = 0$, both (P1) and (P2) reduce to the respective CBF and CoMP BLP design problems considered in our previous work [34].

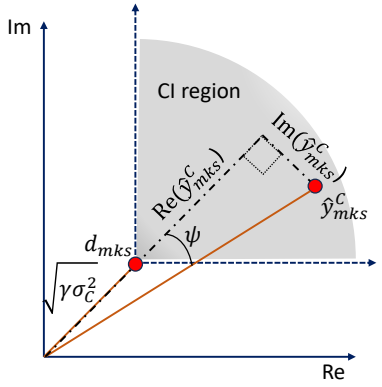

Fig. 2: SLP: the $\langle d_{mks}$ rotated noiseless received signal $\hat{y}_{mks} = \tilde{\mathbf{h}}_{m,mks}^{\mathrm{T}}\mathbf{x}_{ms}d_{mks}$ should fall in the CI region of the transmitted QPSK symbol d_{mks}.

IV. Robust Symbol Level Precoding

In this section, we explain the SLP design framework for CBF and CoMP BS coordination schemes.

A. Overview: SLP

The main idea involves leveraging co-channel interference constructively to increase the received signal power. This is achieved by instantaneously aligning the interfering signals with the desired signal at each receive antenna, as shown in Fig. 2. For a single-cell system, if the s^{th} transmitted symbol is M-PSK-modulated: $d_{mks} = de^{j\phi_{mks}}$, the received signal at U_{mk} can be represented as

$$\begin{aligned} y_{mks}^{\mathrm{C}} &= \tilde{\mathbf{h}}_{m,mk}^{\mathrm{T}}\sum_{l=1}^{K}\mathbf{w}_{ml}d_{mls} + z_{mks}^{\mathrm{C}}, \\ &= \tilde{\mathbf{h}}_{m,mk}^{\mathrm{T}}\sum_{l=1}^{K}\mathbf{w}_{ml}e^{j(\phi_{mls}-\phi_{mks})}d_{mks} + z_{mks}^{\mathrm{C}}, \\ &= \tilde{\mathbf{h}}_{m,mks}^{\mathrm{T}}\mathbf{x}_{ms}d_{mks} + z_{mks}^{\mathrm{C}}, \end{aligned} \tag{56}$$

where $\tilde{\mathbf{h}}_{m,mks}^{\mathrm{T}} = \tilde{\mathbf{h}}_{m,mk}^{\mathrm{T}}e^{j(-\phi_{mks})}$ and $\mathbf{x}_{ms} = \sum_{l=1}^{K}\mathbf{w}_{ml}e^{j(\phi_{mls})}$ (for $d = 1$). Hence, from Fig. 2, the condition for $\mathbf{y}_{mks}^{\mathrm{C}}$ lying in the CI region of d_{mks} to achieve a SINR of γ can be expressed as,

$$|\mathrm{Im}\left(\hat{\mathbf{h}}_{m,mks}^{\mathrm{T}}\mathbf{x}_{ms}\right)| \leq \left(\mathrm{Re}\left(\tilde{\mathbf{h}}_{m,mks}^{\mathrm{T}}\mathbf{x}_{ms} - \sigma_{\mathrm{C}}\sqrt{\gamma}\right)\right)\tan\psi, \tag{57}$$

where, $\psi = \pi/M_{\mathrm{psk}}$. For a detailed discussion about SLP, we refer the readers to [22] and [39].

This article has been accepted for publication in IEEE Transactions on Wireless Communications. This is the author's version which has not been fully edited and content may change prior to final publication. Citation information: DOI 10.1109/TWC.2024.3417713

B. SLP: Coordinated Beamforming

In the CBF case, the s^{th} received symbol at U_{mk} is obtained by extending (56) to a multi-cell scenario as follows:

$$y^{\text{C}}_{mks} = \tilde{\mathbf{h}}^{\text{T}}_{m,mks}\mathbf{x}_{ms}d_{mks} + \sum_{n\neq m}^{J}\tilde{\mathbf{h}}^{\text{T}}_{n,mks}\mathbf{x}_{ns}d_{nks} + \mathbf{z}^{\text{C}}_{mks}, \quad (58)$$

where $\tilde{\mathbf{h}}^{\text{T}}_{n,mks} = \tilde{\mathbf{h}}^{\text{T}}_{n,mk}e^{j(-\phi_{nks})}$ and $\mathbf{x}_{ns} = \sum_{l=1}^{K}\mathbf{w}_{nl}e^{j(\phi_{nls})}$. Since the data symbols are not shared among the BSs in the CBF mode, the SLP design can only align the intra-cell interference to enhance the received signal power, whereas the inter-cell interference degrades the SINR value. Hence, the SINR constraint is equivalently written as a CI constraint given by (60a), where $\gamma^{'} = \sqrt{\gamma}$.

The corresponding problem formulation using SLP is given by

$$(\text{P3}): \underset{\{\mathbf{x}_{ms},\mathbf{R}_{\mathbf{x}_{ms}},t_{m,\text{cbf}},\gamma'\}}{\text{maximize}} \ \frac{t_{m,\text{cbf}}\cdot\rho}{\text{NF}^{\text{slp}}_{\text{R,cbf}}} + \frac{(1-\rho)\cdot\gamma^{'}}{\text{NF}^{\text{slp}}_{\text{C,cbf}}},$$

$$\text{s.t.}\begin{bmatrix} F^{\text{R}}_{\theta_m\theta_m} - t_{m,\text{cbf}} & \mathbf{f}_{\theta_m\boldsymbol{\eta}_{m,\text{cbf}}} \\ \mathbf{f}^{\text{T}}_{\theta_m\boldsymbol{\eta}_{m,\text{cbf}}} & \mathbf{F}_{\boldsymbol{\eta}_{m,\text{cbf}}\boldsymbol{\eta}_{m,\text{cbf}}}\end{bmatrix} \succeq \mathbf{0}, \quad (59a)$$

$$\frac{1}{L}\text{tr}\left(\sum_{s=1}^{L}\mathbf{R}_{\mathbf{X}_{ms}}\right) \leq P_{\text{t}}, \quad (59b)$$

$$\begin{bmatrix}\mathbf{R}_{\mathbf{X}_{ms}} & \mathbf{x}_{ms} \\ \mathbf{x}^{\text{H}}_{ms} & 1\end{bmatrix} \succeq \mathbf{0};\ \mathbf{R}_{\mathbf{X}_{ms}} \succeq \mathbf{0}\ \forall s, \quad (59c)$$

(60a). (59d)

The objective function of (P3) is the weighted combination of minimizing the CRB and maximizing the minimum SINR values. Note that, unlike the BLP design problem (P1), the optimization variables in this context are the transmit symbol vector $\mathbf{x}_{ms}$ and its covariance matrix $\mathbf{R}_{\mathbf{x}_{ms}}$. Additionally, the entries of $\mathbf{F}_{m,\text{cbf}}$ value is a function $\mathbf{R}_{\mathbf{x}_m} = (1/L)\sum_{s=1}^{L}\mathbf{x}_{ms}\mathbf{x}^{\text{H}}_{ms} = (1/L)\sum_{s=1}^{L}\mathbf{R}_{\mathbf{x}_{ms}}$. Similar to (P1), $\text{NF}^{\text{slp}}_{\text{R,cbf}}$ and $\text{NF}^{\text{slp}}_{\text{C,cbf}}$ are determined by solving (P3) for $\rho = 1$ and $\rho = 0$, respectively. Equation (59a) limits the Fisher information value to be less than or equal to $t_{m,\text{cbf}}$ using the Schur complement: $F^{\text{R}}_{\theta_m\theta_m} - \mathbf{f}_{\theta_m\boldsymbol{\eta}_{m,\text{cbf}}}\mathbf{F}_{\boldsymbol{\eta}_{m,\text{cbf}}\boldsymbol{\eta}_{m,\text{cbf}}}\mathbf{f}^{\text{T}}_{\theta_m\boldsymbol{\eta}_{m,\text{cbf}}} >= t_{m.\text{cbf}}$. Equation (59b) is the average power constraint. Equation (59c) is the semi-definite relaxed (SDR) representation of the relation between $\mathbf{R}_{\mathbf{x}_{ms}}$ and $\mathbf{x}_{ms}$ using the Schur complement. Solving (P3) poses challenges stemming from (a) the infinite possibilities of $\mathbf{e}_{mks}$ in (60a), (b) the non-convex multiplication between $\gamma^{'}$ and the interference terms in (60a) and (c) the non-convex form of $\mathbf{C}_{m,\text{cbf}}$ in (59a).

To tackle (a) and (b), let $\tilde{\mathbf{h}}_{m,mks} = \tilde{\mathbf{h}}^{\text{R}}_{m,mks} + j\tilde{\mathbf{h}}^{\text{I}}_{m,mks} = \mathbf{h}^{\text{R}}_{m,mks} + j\mathbf{h}^{\text{I}}_{m,mks} + \mathbf{e}^{\text{R}}_{mks} + j\mathbf{e}^{\text{I}}_{mks}$, then

$$\text{Im}\left\{\tilde{\mathbf{h}}^{\text{T}}_{m,mks}\mathbf{x}_{ms}\right\} = \hat{\mathbf{f}}^{\text{T}}_{m,mks}\hat{\mathbf{x}}_{ms} + \hat{\mathbf{e}}^{\text{T}}_{mks}\hat{\mathbf{x}}_{ms}, \quad (61)$$

$$\text{Re}\left\{\tilde{\mathbf{h}}^{\text{T}}_{m,mks}\mathbf{x}_{ms}\right\} = \hat{\mathbf{f}}^{\text{T}}_{m,mks}\hat{\mathbf{x}}^{'}_{ms} + \hat{\mathbf{e}}^{\text{T}}_{mks}\hat{\mathbf{x}}^{'}_{ms}, \quad (62)$$

where $\hat{\mathbf{f}}_{m,mks} = \left[\mathbf{h}^{\text{R}}_{m,mks};\mathbf{h}^{\text{I}}_{m,mks}\right]$, $\hat{\mathbf{e}}_{mks} = \left[\mathbf{e}^{\text{R}}_{mks};\mathbf{e}^{\text{I}}_{mks}\right]$, $\hat{\mathbf{x}}_{ms} = \left[\mathbf{x}^{\text{I}}_{ms};\mathbf{x}^{\text{R}}_{ms}\right]$, and $\hat{\mathbf{x}}^{'}_{ms} = \left[\mathbf{x}^{\text{R}}_{ms};-\mathbf{x}^{\text{I}}_{ms}\right]$. Then (60a) can be equivalently expressed as (60b) and (60c). Taking the maximum value of the LHS, the constraints are equal to,

$$\hat{\mathbf{f}}^{\text{T}}_{m,mks}\hat{\mathbf{x}}_{ms} - \hat{\mathbf{f}}^{\text{T}}_{m,mks}\hat{\mathbf{x}}^{'}_{ms}\text{tan}\psi + \gamma^{'}\sqrt{\sigma^2_{\text{C}} + I^{2\text{inter}}_{\text{sl,cbf}}}\text{tan}\psi + \delta\|\hat{\mathbf{x}}_{ms} - \hat{\mathbf{x}}^{'}_{ms}\text{tan}\psi\| \leq 0, \quad (63)$$

$$-\hat{\mathbf{f}}^{\text{T}}_{m,mks}\hat{\mathbf{x}}_{ms} - \hat{\mathbf{f}}^{\text{T}}_{m,mks}\hat{\mathbf{x}}^{'}_{ms}\text{tan}\psi + \gamma^{'}\sqrt{\sigma^2_{\text{C}} + I^{2\text{inter}}_{\text{sl,cbf}}}\text{tan}\psi + \delta\|\hat{\mathbf{x}}_{ms} + \hat{\mathbf{x}}^{'}_{ms}\text{tan}\psi\| \leq 0, \quad (64)$$

where $I^{2\text{inter}}_{\text{sl,cbf}}$ is the maximum ICI that satisfies

$$\max_{\|\mathbf{e}_{nks}\|^2\leq\delta^2}\|\tilde{\mathbf{h}}^{\text{T}}_{m,nks}\mathbf{x}_{ms}\|^2 \leq \frac{I^{2\text{inter}}_{\text{sl,cbf}}}{J-1}. \quad (65)$$

Note that the squared representation of ICI: $I^{2\text{inter}}_{\text{sl,cbf}}$, is to ensure convexity for the constraints (63) and (64). Using Cauchy-Schwarz inequality, we have

$$\left(\|\mathbf{h}^{\text{T}}_{m,nks} + \mathbf{e}^{\text{T}}_{nks}\right)\mathbf{x}_{ms}\|^2 \leq \left(\|\mathbf{h}^{\text{T}}_{m,nks}\mathbf{x}_{ms}\| + \|\mathbf{e}^{\text{T}}_{nks}\mathbf{x}_{ms}\|\right)^2. \quad (66)$$

Hence, (65) is equivalently written as

$$\|\mathbf{h}^{\text{T}}_{m,nks}\mathbf{x}_{ms}\| + \delta\|\mathbf{x}_{ms}\| \leq \frac{I^{\text{inter}}_{\text{sl,cbf}}}{\sqrt{J-1}}. \quad (67)$$

Note that for a given $I^{\text{inter}}_{\text{sl,cbf}}$, the constraints (63), (64), and (67) that combined represent the SINR constraint are convex. Finally, given $\{\mathbf{R}_{\mathbf{X}_n}\}$, the estimation of $\mathbf{C}_{m,\text{cbf}}$ can be achieved using (9). This makes the entries of $\mathbf{F}_{m,\text{cbf}}$ in (59a) an affine function of $\mathbf{R}_{\mathbf{X}_m}$.

Hence, we solve (P3) by solving the following two optimization problems alternatively untill convergence:

$$(\text{P3.A}): \underset{\{\mathbf{x}_{ms},\mathbf{R}_{\mathbf{x}_{ms}},t_{m,\text{cbf}},\gamma'\}}{\text{maximize}} \ \frac{t_{m,\text{cbf}}\cdot\rho}{\text{NF}^{\text{slp}}_{\text{R,cbf}}} + \frac{(1-\rho)\cdot\gamma^{'}}{\text{NF}^{\text{slp}}_{\text{C,cbf}}},$$

$$\text{s.t.(59a)} - \text{(59c)}, (63), (64), (67); \quad (68a)$$

$$(\text{P3.B}): \underset{\{\mathbf{x}_{ms},\mathbf{R}_{\mathbf{x}_{ms}},I^{2\text{inter}}_{m,\text{sl,cbf}}\}}{\text{minimize}} \ I^{2\text{inter}}_{m,\text{sl,cbf}},$$

$$\text{s.t.}\begin{bmatrix} F^{\text{R}}_{\theta_m\theta_m} - t^{*}_{m,\text{cbf}} & \mathbf{f}_{\theta_m\boldsymbol{\eta}_{m,\text{cbf}}} \\ \mathbf{f}^{\text{T}}_{\theta_m\boldsymbol{\eta}_{m,\text{cbf}}} & \mathbf{F}_{\boldsymbol{\eta}_{m,\text{cbf}}\boldsymbol{\eta}_{m,\text{cbf}}}\end{bmatrix} \succeq \mathbf{0}, \quad (69a)$$

$$\hat{\mathbf{f}}^{\text{T}}_{m,mks}\hat{\mathbf{x}}_{ms} - \hat{\mathbf{f}}^{\text{T}}_{m,mks}\hat{\mathbf{x}}^{'}_{ms}\text{tan}\psi + \gamma^{'*}\sqrt{\sigma^2_{\text{C}} + I^{2\text{inter}}_{\text{sl,cbf}}}\text{tan}\psi + \delta\|\hat{\mathbf{x}}_{ms} - \hat{\mathbf{x}}^{'}_{ms}\text{tan}\psi\| \leq 0, \quad (69b)$$

$$-\hat{\mathbf{f}}^{\text{T}}_{m,mks}\hat{\mathbf{x}}_{ms} - \hat{\mathbf{f}}^{\text{T}}_{m,mks}\hat{\mathbf{x}}^{'}_{ms}\text{tan}\psi + \gamma^{'*}\sqrt{\sigma^2_{\text{C}} + I^{2\text{inter}}_{\text{sl,cbf}}}\text{tan}\psi + \delta\|\hat{\mathbf{x}}_{ms} + \hat{\mathbf{x}}^{'}_{ms}\text{tan}\psi\| \leq 0, \quad (69c)$$

$$\|\mathbf{h}^{\text{T}}_{m,nks}\mathbf{x}_{ms}\| + \delta\|\mathbf{x}_{ms}\| \leq \frac{I^{\text{inter}}_{m,\text{sl,cbf}}}{\sqrt{J-1}}, \quad (69d)$$

$$I^{\text{inter}}_{m,\text{sl,cbf}} <= I^{\text{inter}}_{\text{sl,cbf}}, \text{(59a)} - \text{(59c)}. \quad (69e)$$

Problem (P3.A) maximizes the objective function of (P3) for given $I^{\text{inter}}_{\text{sl,cbf}}$ value. In (P3.B), we minimize the leakage power to the neighbouring cells' users while guaranteeing given sensing ($t_{m,\text{cbf}}$) and communication performance ($\gamma^{'*}$) through (69a)-(69d). The value of the constant $I^{\text{inter}}_{\text{sl,cbf}}$ is given

This article has been accepted for publication in IEEE Transactions on Wireless Communications. This is the author's version which has not been fully edited and content may change prior to final publication. Citation information: DOI 10.1109/TWC.2024.3417713

$$\max_{\|\mathbf{e}_{mks}\|^2\le\delta^2}\left(\left|\mathrm{Im}\left\{\tilde{\mathbf{h}}_{m,mks}^{\mathrm{T}}\mathbf{x}_{ms}\right\}\right|-\left(\mathrm{Re}\left\{\tilde{\mathbf{h}}_{m,mks}^{\mathrm{T}}\mathbf{x}_{ms}\right\}\right)\tan\psi+\gamma^{'}\left(\sqrt{\left(\sigma_{\mathrm{C}}^2+\sum_{n\neq m}^{J}|\tilde{\mathbf{h}}_{n,mks}^{\mathrm{T}}\mathbf{x}_{ns}|^2\right)}\right)\tan\psi\right)\le 0\;\forall k,s \tag{60a}$$

$$\max_{\|\mathbf{e}_{mks}\|^2\le\delta^2}\left(\hat{\mathbf{f}}_{m,mks}^{\mathrm{T}}\hat{\mathbf{x}}_{ms}-\hat{\mathbf{f}}_{m,mks}^{\mathrm{T}}\hat{\mathbf{x}}_{ms}^{'}\tan\psi+\gamma^{'}\left(\sqrt{\left(\sigma_{\mathrm{C}}^2+\sum_{n\neq m}^{J}|\tilde{\mathbf{h}}_{n,mks}^{\mathrm{T}}\mathbf{x}_{ns}|^2\right)}\right)\tan\psi+\hat{\mathbf{e}}_{mks}(\hat{\mathbf{x}}_{ms}-\hat{\mathbf{x}}_{ms}^{'}\tan\psi)\right)\le 0 \tag{60b}$$

$$\max_{\|\mathbf{e}_{mks}\|^2\le\delta^2}\left(-\hat{\mathbf{f}}_{m,mks}^{\mathrm{T}}\hat{\mathbf{x}}_{ms}-\hat{\mathbf{f}}_{m,mks}^{\mathrm{T}}\hat{\mathbf{x}}_{ms}^{'}\tan\psi+\gamma^{'}\left(\sqrt{\left(\sigma_{\mathrm{C}}^2+\sum_{n\neq m}^{J}|\tilde{\mathbf{h}}_{n,mks}^{\mathrm{T}}\mathbf{x}_{ns}|^2\right)}\right)\tan\psi+\hat{\mathbf{e}}_{mks}(-\hat{\mathbf{x}}_{ms}-\hat{\mathbf{x}}_{ms}^{'}\tan\psi)\right)\le 0 \tag{60c}$$

by the maximum of $\{I_{m,\mathrm{sl,cbf}}^{\mathrm{inter}}\}$. The corresponding precoder design procedure is similar to Steps 8 and 9 of Algorithm 1.

C. SLP: Coordinated Multipoint

In the CoMP mode, the s^{th} received symbol at U_k is given by

$$y_{ks}^{\mathrm{C}}=\tilde{\mathbf{h}}_{ks}^{\mathrm{T}}\mathbf{x}_s d_{ks}+\mathbf{z}_{ks}^{\mathrm{C}}, \tag{70}$$

where $\tilde{\mathbf{h}}_{ks}^{\mathrm{T}}=\tilde{\mathbf{h}}_{k}^{\mathrm{T}}e^{j(-\phi_{ks})}$ and $\mathbf{x}_s=\sum_{l=1}^{JK}\mathbf{w}_l e^{j(\phi_{ls})}$. Since the data is shared among the BSs, all the interfering signal power can be aligned with the useful signal power. Hence, the SINR constraint in the CoMP mode, derived from (63) and (64), can be written as

$$\hat{\mathbf{f}}_{ks}^{\mathrm{T}}\hat{\mathbf{x}}_s-\hat{\mathbf{f}}_{ks}^{\mathrm{T}}\hat{\mathbf{x}}_s^{'}\tan\psi+\gamma^{'}\sigma_{\mathrm{C}}\tan\psi+\delta\|\hat{\mathbf{x}}_s-\hat{\mathbf{x}}_s^{'}\tan\psi\|\le 0, \tag{71}$$

$$-\hat{\mathbf{f}}_{ks}^{\mathrm{T}}\hat{\mathbf{x}}_s-\hat{\mathbf{f}}_{ks}^{\mathrm{T}}\hat{\mathbf{x}}_s^{'}\tan\psi+\gamma^{'}\sigma_{\mathrm{C}}\tan\psi+\delta\|\hat{\mathbf{x}}_s+\hat{\mathbf{x}}_s^{'}\tan\psi\|\le 0, \tag{72}$$

where $\tilde{\mathbf{h}}_{ks}^{\mathrm{T}}=\tilde{\mathbf{h}}_{ks}^{\mathrm{R}}+j\tilde{\mathbf{h}}_{ks}^{\mathrm{I}}=\mathbf{h}_{ks}^{\mathrm{R}}+j\mathbf{h}_{ks}^{\mathrm{I}}+\mathbf{e}_{ks}^{\mathrm{R}}+j\mathbf{e}_{ks}^{\mathrm{I}}$ and $\mathbf{x}_s=\sum_{l=1}^{2K}\mathbf{w}_l e^{j(\phi_{ls})}$; $\hat{\mathbf{f}}_{ks}=\left[\mathbf{h}_{ks}^{\mathrm{R}};\mathbf{h}_{ks}^{\mathrm{I}}\right]$, $\hat{\mathbf{e}}_{ks}=\left[\mathbf{e}_{ks}^{\mathrm{R}};\mathbf{e}_{ks}^{\mathrm{I}}\right]$, $\hat{\mathbf{x}}_s=\left[\mathbf{x}_s^{\mathrm{I}};\mathbf{x}_s^{\mathrm{R}}\right]$, and $\hat{\mathbf{x}}_s^{'}=\left[\mathbf{x}_s^{\mathrm{R}};-\mathbf{x}_s^{\mathrm{I}}\right]$. The corresponding optimization problem is formulated as,

$$(\mathrm{P4}):\underset{\{\mathbf{x}_s,\mathbf{R}_{\mathbf{x}_s},f,\gamma'\}}{\text{maximize}}\;\frac{f\cdot\rho}{\mathrm{NF}_{\mathrm{R,comp}}^{\mathrm{slp}}}+\frac{(1-\rho)\cdot\gamma^{'}}{\mathrm{NF}_{\mathrm{C,comp}}^{\mathrm{slp}}},$$

$$\text{s.t.}\begin{bmatrix}F_{\theta_m\theta_m}^{\mathrm{R}}-t_{m,\mathrm{comp}} & \mathbf{f}_{\theta_m\boldsymbol{\eta}_{m,\mathrm{comp}}}\\ \mathbf{f}_{\theta_m\boldsymbol{\eta}_{m,\mathrm{comp}}}^{\mathrm{T}} & \mathbf{F}_{\boldsymbol{\eta}_{m,\mathrm{comp}}\boldsymbol{\eta}_{m,\mathrm{comp}}}\end{bmatrix}\succeq\mathbf{0}, \tag{73a}$$

$$t_{m,\mathrm{comp}}\ge f,\quad\forall m, \tag{73b}$$

$$\begin{bmatrix}\mathbf{R}_{\mathbf{X}_s} & \mathbf{x}_s\\ \mathbf{x}_s^{\mathrm{H}} & 1\end{bmatrix}\succeq\mathbf{0}\;\forall s\;\mathbf{R}_{\mathbf{X}_s}\succeq\mathbf{0}, \tag{73c}$$

$$\frac{1}{L}\mathrm{tr}\left(\mathbf{D}_m\sum_{s=1}^{L}\mathbf{R}_{\mathbf{X}_s}\mathbf{D}_m^{'}\right)\le P_{\mathrm{t}}, \tag{73d}$$

$$(71),(72). \tag{73e}$$

Problem (P4) maximizes the same objective as (P2). Here, (73a), (73b), and (73d) are the same as (49a), (49b), and (49d). The convex optimization problem (P4) can be solved using Matlab's CVX [38]. Due to the SDR in (P3.A) and (P4): $\mathbf{R}_{\mathbf{X}_s}\succeq\mathbf{x}_s\mathbf{x}_s^{\mathrm{H}}$, the obtained objective values represent the upper bound. Moreover, by setting $\rho=0$, (P3) and (P4) can be modified to the SLP design formulations, Eq. (16) and Eq. (39), in [35] where the objective was to minimize the total power subject to a minimum SINR constraint.

V. Convergence, Complexity, and Overhead Analysis

As explained in Sections III and IV, the robust precoders for CBF-BLP, CoMP-BLP, and CBF-SLP are obtained using the AO algorithm given in Algorithm 1. Recall the AO algorithm employed alternates between optimizing precoders to maximize the weighted combination of sensing and communication performance metrics under specified maximum interference values, and minimizing communication and sensing interference values while ensuring given sensing and communication performance thresholds. The convergence of such an iterative algorithm is proven in [40], and we also show it empirically in Fig. 6.

The optimization problems that give the robust precoders: (P1.1.A), (P1.1.B), (P2.1.A), (P2.1.B), (P3.A), (P3.B), and (P4) are convex optimization problems obtained through SDR technique which can be solved using Algorithm 1. Since there is no closed-form expression for the iterative complexity of SDP optimization, we give the time complexity of each iteration of Algorithm 1 solved using interior point methods. If V is the number of variables, and C is the number of constraints, then the computational complexity in time is

$$C_{\mathrm{t}}\sim\mathcal{O}(\sqrt{V}(CV^2+C^{2.7}+V^{2.7})\log(1/\epsilon)), \tag{74}$$

a polynomial function of V and C with ϵ being the relative accuracy [41]. Note that BLP optimizations ((P1.A), (P1.B), (P2.A), (P2.B)) have low computational complexity compared to the SLP optimization ((P3.A), (P3.B), and (P4)) since the number of constraints of the later increases with the length of the communication frame. However, the receiver complexity at the user end in the SLP cases is low since it leverages the co-channel interference constructively. The primary advantage of utilizing SLP lies in its ability to offer a solution with a small number of antennas. In contrast, the performance of the BLP scheme is limited by increased intra-cell interference when the number of antennas is limited.

The total overhead of sharing CSI and user data amongst J BSs in CoMP mode is

$$O_{\mathrm{CoMP}}\sim\mathcal{O}(J(J-1)(K(J\beta_{\mathrm{h}}+\beta_{\mathrm{S}})), \tag{75}$$

where β_{h} is the number of bits required to represent CSI from a BS to a user, and β_{S} represents bits required to exchange user's data. The overhead associated with the CBF mode is

$$O_{\mathrm{CoMP}}\sim\mathcal{O}(J(J-1)(K(J\beta_{\mathrm{h}})), \tag{76}$$

This article has been accepted for publication in IEEE Transactions on Wireless Communications. This is the author's version which has not been fully edited and content may change prior to final publication. Citation information: DOI 10.1109/TWC.2024.3417713

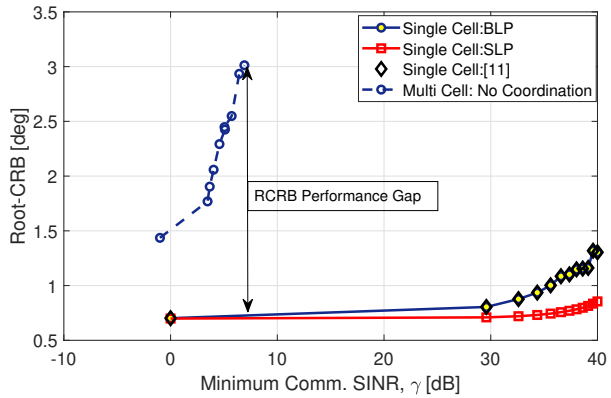

Fig. 3: RCRB Vs minimum SINR performance when $N_{\mathrm{tx}} = 10$, $N_{\mathrm{rx}} = 10$, $K = 3$, $\delta = 0$, $M_{\mathrm{psk}} = 4$, $P_{\mathrm{t}}/\sigma_{\mathrm{C}}^2 = P_{\mathrm{t}}/\sigma_{\mathrm{R}}^2 = 40$ dB. Single-cell solutions in the proximity of additional BSs are sub-optimal, motivating exploration of multi-cell ISAC setups.

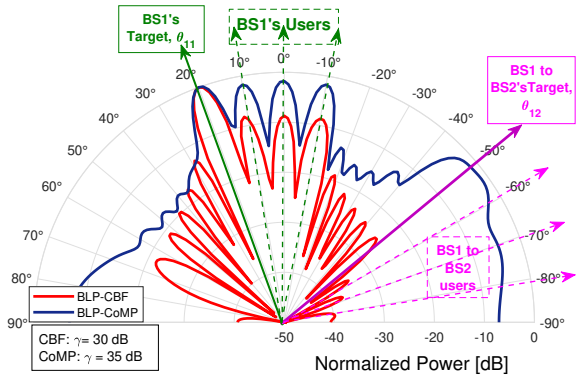

Fig. 4: Final beampattern for BS1, when $J = 2$, CBF, $\gamma = 30$ dB, CoMP, $\gamma = 35$ dB $N_{\mathrm{tx}} = 20$, $N_{\mathrm{rx}} = 15$, $K = 3$, $\delta = 0.01$,$M_{\mathrm{psk}} = 4$.

and is relatively lower due to the non-exchange of user data amongst BSs. Moreover, the CoMP scheme requires precise synchronization among BSs and operates optimally when all BSs establish LoS links with all intended targets.

VI. Numerical Evaluation

In this section, we present our main findings through numerical evaluations. The simulation parameters are $K = 3$, $P_{\mathrm{t}}/\sigma_{\mathrm{C}}^2 = P_{\mathrm{t}}/\sigma_{\mathrm{R}}^2 = 30$ dB, and $f_c = 5.6$ GHz. The communication channel gains are normalized such that the signal power received through an inter-cell link is considered to be reduced by a factor of 3. α_m is selected such that the received SNR of the intra-cell echo signal: $|\alpha_m|^2 L P_{\mathrm{t}}/\sigma_{\mathrm{R}}^2 = 1$ [11], whereas $|\alpha_n|^2 = |\alpha_m|^2/3$. The ratio of the maximum tolerable interference values to the noise power is selected as 10 dB.

Fig. 3 shows the effect of neglecting the inter-cell links in a multi-cell ISAC system that uses BLP. The plots between the root CRB (RCRB) and the minimum SINR experienced by a communication user are obtained by solving (P1.A), neglecting the inter-cell links and assuming no CSI error. Then, the obtained precoders are used to determine the actual sensing versus communication performance trade-off. As seen

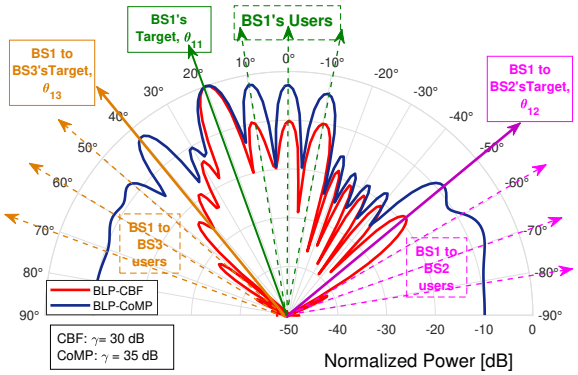

Fig. 5: Final beampattern for BS1, when $J = 3$,CBF, $\gamma = 30$ dB, CoMP, $\gamma = 35$ dB $N_{\mathrm{tx}} = 20$, $N_{\mathrm{rx}} = 20$, $K = 3$, $\delta = 0.01$,$M_{\mathrm{psk}} = 4$.

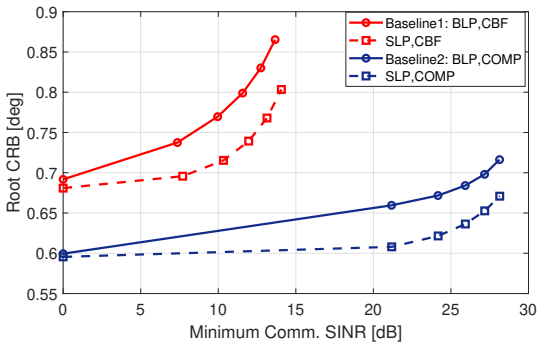

Fig. 6: RCRB Vs. comm SINR threshold when, $N_{\mathrm{tx}} = 6$, $N_{\mathrm{rx}} = 10$, $K = 3$, $\delta = 0.01$, $M_{\mathrm{psk}} = 4$.

in the figure, the additional signal power received through the inter-cell links can negatively affect both the sensing and the communication performances. This motivates us to consider a multi-cell ISAC setup since the single-cell solutions are suboptimal when additional BSs are deployed in proximity. Moreover, in a single-cell setup, the derived CRB expression matches with that in [11].

Figs. 4 and 5 show the final transmit beampattern obtained using BLP applied to CBF and CoMP multi-cell scenarios. For better analysis, we assume the users are in LoS with the BSs along the directions marked in the figure.

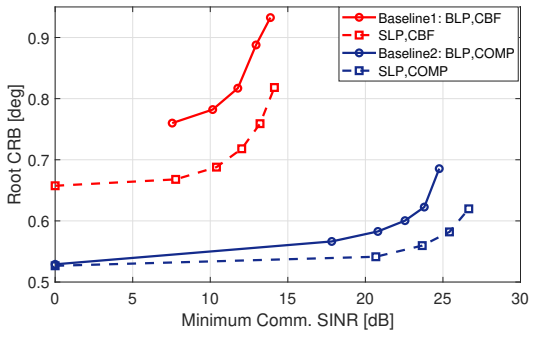

Fig. 7: RCRB Vs. comm SINR threshold when, $J = 3$,$N_{\mathrm{tx}} = 6$, $N_{\mathrm{rx}} = 10$, $K = 3$, $\delta = 0.01$, $M_{\mathrm{psk}} = 4$.

This article has been accepted for publication in IEEE Transactions on Wireless Communications. This is the author's version which has not been fully edited and content may change prior to final publication. Citation information: DOI 10.1109/TWC.2024.3417713

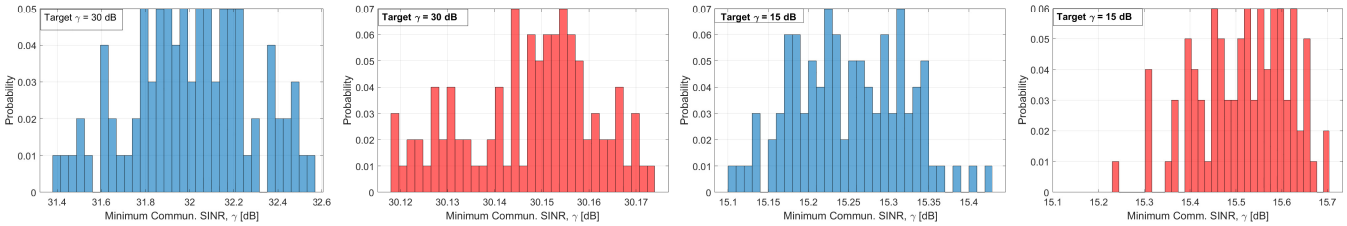

(a) BLP CoMP. (b) SLP CoMP. (c) BLP CBF. (d) SLP CBF.

Fig. 8: Probability distribution of observed minimum SINR for 100 different error vector realization, when γ = 30 dB (CoMP),γ = 15 dB (CBF) $N_{\text{tx}} = 16$, $N_{\text{rx}} = 6$, $\delta = 0.01$, $M_{\text{psk}} = 4$, $J = 2$.

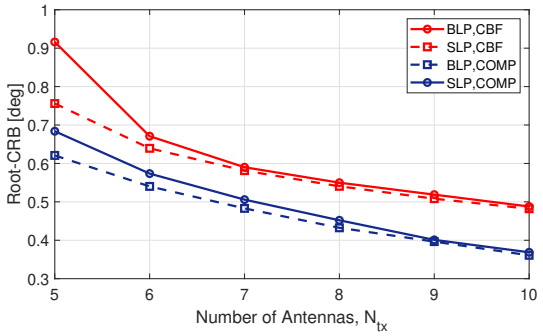

Fig. 9: Variation of RCRB w.r.t the number of transmit antennas, when γ = 10 dB, $N_{\text{rx}} = 10$, $K = 3$, $\delta = 0.01$, $M_{\text{psk}} = 4$.

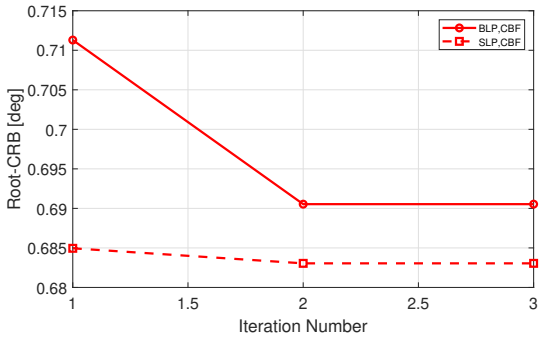

Fig. 10: Convergence of Algorithm 1 when γ = 10 dB, $N_{\text{tx}} = 10$, $N_{\text{rx}} = 6$, $K = 3$, $\delta = 0.01$, $M_{\text{psk}} = 4$.

The beampatterns are obtained for a 2-cell and 3-cell ISAC system, respectively. Specifically, for the m^{th}, BS operating in CBF mode, the beampattern is plotted using the formula $\mathbf{b}^{\text{T}}(\theta)\mathbf{R}_{\mathbf{X}_m}\mathbf{b}^{*}(\theta)$ where $\mathbf{b}(\theta) \in \mathcal{C}^{N_{\text{tx}}\times 1}$ is the array steering vector in direction θ and $\mathbf{R}_{\mathbf{X}_m} = \sum_{k=1}^{K} \mathbf{w}_k\mathbf{w}_k^{\text{H}}$ is obtained from Algorithm 1. Correspondingly, the CoMP mode beampattern is obtained using $\mathbf{b}^{'\text{T}}(\theta)\mathbf{D}_m\mathbf{R}_{\mathbf{X}}\mathbf{D}_m^{'}\mathbf{b}^{'*}(\theta)$, with $\mathbf{b}^{'}(\theta) = \{\vec{0}_{N_{\text{tx}}}, .., \mathbf{b}(\theta), .., \vec{0}_{N_{\text{tx}}}\} \in \mathcal{C}^{N\times 1}$. As seen in the figures, for the CBF scheme, the power radiated towards the neighbouring BSs' users/targets through the sensing and the communication links is low compared to the CoMP scheme. This is because the inter-cell links degrade the sensing and communication performances in the CBF scheme due to the non-sharing of the user data among the BSs. On the other hand, the CoMP scenario improves the ISAC performance by radiating more power through the inter-cell links, where it jointly serves the communication users while offering bi-static sensing. Furthermore, Comparing the beampatterns of a 2-cell (Fig. 4) and 3-cell system (Fig. 5), with the inclusion of a third BS, the CoMP precoder solution directs power towards the inter-cell communication and sensing directions of the third cell. In contrast, the CBF scheme shows minimal power radiation in those directions. These findings affirm the applicability of the proposed model to scenarios involving more than two BSs..

Figs. 6 and 7 show the RCRB- γ trade-off for the considered four scenarios: BLP-CBF, BLP-CoMP, SLP-CBF, and SLP-CoMP, when $\delta = 0.01$. The plots in Fig. 6 are done by averaging the obtained results over 20 different target and user positions. Recall that, in [34], we examined BLP-CBF and BLP-CoMP under $\delta = 0$. These solutions serve as benchmarks against their SLP counterparts. In all the plots, the sensing error performance remains relatively low in the low γ regime since the BS can meet the communication performance without sacrificing the power radiated towards the target. As the communication performance demand increases, the power radiated towards the target is reduced to meet the demand, thereby negatively affecting the sensing performance. As seen in the figures, the SLP technique outperforms the BLP counterparts: in the CBF scenario, the SLP technique utilizes the intra-cell interference constructively, thereby reducing the power needed to achieve the minimum SINR compared to the BLP technique, thus allowing the BS to radiate more power towards its target to improve the sensing performance. In the CoMP case, firstly, there is an improvement in the sensing error due to the multi-static sensing. Moreover, the inter-cell links are constructively utilized by the BLP technique to outperform the BLP-CBF scheme; however, it still suffers from the intra-cell interference while the SLP further improves the ISAC performance utilizing both the intra-cell and inter-cell interference. Furthermore, the high-SINR regime characterizes the sensing performance achieved by precoder solutions primarily designed for communication, similar to the approach explored in [35].

In Figs. 8a-8d, we show the robustness of the obtained solution against the CSI error when $\delta = 0.01$. The observed minimum SINR's probability distributions are obtained after 100 realizations of the error vector. As seen in the figure, all the observed minimum SINR values are above the set thresholds (15 dB for CBF and 30 dB for CoMP), which

This article has been accepted for publication in IEEE Transactions on Wireless Communications. This is the author's version which has not been fully edited and content may change prior to final publication. Citation information: DOI 10.1109/TWC.2024.3417713

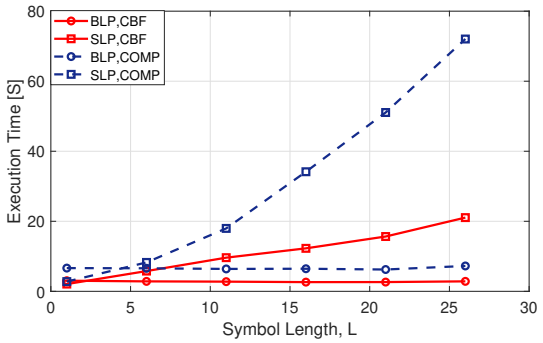

Fig. 11: The effect of symbol length on the execution time of the proposed BLP and SLP schemes when $\gamma = 10$ dB, $N_{\text{tx}} = 10$, $N_{\text{rx}} = 6$, $K = 3$, $\delta = 0.01$, $M_{\text{psk}} = 4$.

shows that the minimum SINR constraint is satisfied under worst-case scenarios.

Fig. 9 shows the effect of the number of transmitting antennas on the sensing performance for a given minimum communication SINR of 10 dB. The broader beamwidth associated with a lower number of transmit antennas increases the interference to the users demanding more power to achieve the required SINR value. This causes a poorer sensing performance than with more antennas at the transmitting end.

Fig. 10 shows the convergence of Algorithm 1 in terms of the while-loop iterations required. The RCRB value decreases as the iteration progresses, reaching a steady value in 2 iterations for the considered simulation parameters. The choice of $I_{m,\text{cbf}}^{\text{intra}}$, $I_{\text{cbf}}^{\text{inter}}$, I_{comp} plays an important role in the convergence speed and the final RCRB value: a higher value requires more number of iterations, whereas, a lower value restricts the complete usage of the available power budget to decrease the interference caused. This would result in a high RCRB value, hence a high target parameter estimation error.

Fig. 11 shows the effect of symbol length (L) on the execution time of considered BLP and SLP schemes. The execution times marked in the figure are obtained using a 12th Gen Intel(R) Core(TM) i7-1265U 1.80 GHz processor with a memory capacity of 32.0 GB RAM (31.7 GB usable). As seen in the figure, the symbol length has a direct impact on the complexity and execution time of the SLP schemes since the number of constraints and optimization variables of (P3) and (P4) increase with L. Moreover, it's worth noting that adopting a block-level approach, as proposed in [42], can mitigate the complexity and overhead associated with SLP.

VII. Conclusion

In this work, we considered robust precoding techniques for coordinated beamforming (CBF) and coordinated multi-point (CoMP) multi-cell scenarios of a multi-user multi-input-single-output (MISO) integrated sensing and communication (ISAC) networks. We derived the Cramer-Rao bound (CRB) expressions of the considered multi-cell scenarios, whose inverse gives the lower bound on the estimation error variance. Using the derived expressions, we formulated precoder design problems that minimize CRB and maximize the minimum communication signal-to-noise-plus-interference ratio (SINR) subject to a total power constraint. The design considered both the block-level and symbol-level precoding techniques, and the non-convexity of the problems were tackled by a combination of semidefinite relaxation (SDR) and alternating optimization (AO) techniques. As the first work to consider robust precoding techniques for a multi-cell ISAC system, we initially investigated the effect of additional signal power received through inter-cell links. As such, we deduced that if not carefully considered, the inter-cell sensing and communication links reduce the sensing accuracy while decreasing the received SINR. Among the considered multi-cell scenarios, the CoMP performs well in terms of both sensing accuracy and communication SINR, compared to the CBF scenario, since it uses the leaked power from the neighbouring BSs constructively for multi-static sensing and for boosting the serving users' SINRs. Additionally, in both the multi-cell scenarios, the SLP solution outperformed the BLP counterpart due to its ability to use the co-channel interference constructively.

References

[1] F. Liu, C. Masouros, A. P. Petropulu, H. Griffiths, and L. Hanzo, "Joint Radar and Communication Design: Applications, State-of-the-Art, and the Road Ahead," *IEEE Trans. on Commun.*, vol. 68, no. 6, pp. 3834–3862, 2020.

[2] F. Liu, Y. Cui, C. Masouros, J. Xu, T. X. Han, Y. C. Eldar, and S. Buzzi, "Integrated sensing and communications: Toward dual-functional wireless networks for 6G and beyond," *IEEE journal on selected areas in communications*, vol. 40, no. 6, pp. 1728–1767, 2022.

[3] W. Chen, X. Lin, J. Lee, A. Toskala, S. Sun, C. F. Chiasserini, and L. Liu, "5g-advanced toward 6g: Past, present, and future," *IEEE Journal on Selected Areas in Communications*, vol. 41, no. 6, pp. 1592–1619, 2023.

[4] I. T. Union, "Future Technology Trends of Terrestrial International Mobile Telecommunications Systems Towards 2030 and Beyond," 2022.

[5] A. Kaushik, R. Singh, S. Dayarathna, R. Senanayake, M. Di Renzo, M. Dajer, H. Ji, Y. Kim, V. Sciancalepore, A. Zappone *et al.*, "Towards Integrated Sensing and Communications for 6G: A Standardization Perspective," *arXiv preprint arXiv:2308.01227*, 2023.

[6] K. Meng, Q. Wu, S. Ma, W. Chen, K. Wang, and J. Li, "Throughput Maximization for UAV-Enabled Integrated Periodic Sensing and Communication," *IEEE Trans. on Wireless Commun.*, vol. 22, no. 1, pp. 671–687, 2023.

[7] F. Liu, L. Zhou, C. Masouros, A. Li, W. Luo, and A. Petropulu, "Toward Dual-Functional Radar-Communication Systems: Optimal Waveform Design," *IEEE Trans. on Signal Processing*, vol. 66, no. 16, pp. 4264–4279, 2018.

[8] C. Sturm and W. Wiesbeck, "Waveform Design and Signal Processing Aspects for Fusion of Wireless Communications and Radar Sensing," *Proceedings of the IEEE*, vol. 99, no. 7, pp. 1236–1259, 2011.

[9] D. Ma, N. Shlezinger, T. Huang, Y. Shavit, M. Namer, Y. Liu, and Y. C. Eldar, "A hardware prototype for joint radar-communication system using spatial modulation," in *2021 55th Asilomar Conference on Signals, Systems, and Computers*, 2021, pp. 634–639.

[10] M. Temiz, C. Horne, N. J. Peters, M. A. Ritchie, and C. Masouros, "An Experimental Study of Radar-Centric Transmission for Integrated Sensing and Communications," *IEEE Trans. on Microwave Theory and Techniques*, 2023.

[11] F. Liu, Y.-F. Liu, A. Li, C. Masouros, and Y. C. Eldar, "Cramér-Rao Bound Optimization for Joint Radar-Communication Beamforming," *IEEE Transactions on Signal Processing*, vol. 70, pp. 240–253, 2021.

[12] X. Liu, T. Huang, N. Shlezinger, Y. Liu, J. Zhou, and Y. C. Eldar, "Joint Transmit Beamforming for Multiuser MIMO Communications and MIMO Radar," *IEEE Trans. on Signal Processing*, vol. 68, pp. 3929–3944, 2020.

[13] X. Yuan, Z. Feng, J. A. Zhang, W. Ni, R. P. Liu, Z. Wei, and C. Xu, "Spatio-Temporal Power Optimization for MIMO Joint Communication and Radio Sensing Systems With Training Overhead," *IEEE Transactions on Vehicular Technology*, vol. 70, no. 1, pp. 514–528, 2021.

[14] B. Li and A. P. Petropulu, "Joint Transmit Designs for Coexistence of MIMO Wireless Communications and Sparse Sensing Radars in Clutter," *IEEE Trans. on Aerospace and Electronic Systems*, vol. 53, no. 6, pp. 2846–2864, 2017.

[15] M. Temiz, E. Alsusa, and M. W. Baidas, "Optimized Precoders for Massive MIMO OFDM Dual Radar-Communication Systems," *IEEE Trans. on Commun.*, vol. 69, no. 7, pp. 4781–4794, 2021.

[16] T. Xu, F. Liu, C. Masouros, and I. Darwazeh, "Proof of Concept experiments of Joint Waveform Design for Integrated Sensing and Communications," in *Proceedings of the 1st ACM MobiCom Workshop on Integrated Sensing and Communications Systems*, 2022, pp. 25–30.

[17] C. D. Ozkaptan, H. Zhu, E. Ekici, and O. Altintas, "Software-Defined MIMO OFDM Joint Radar-Communication Platform with Fully Digital mmWave Architecture," in *2023 IEEE 3rd International Symposium on Joint Communications & Sensing (JC&S)*. IEEE, 2023, pp. 1–6.

[18] Z. Liao, F. Liu, A. Li, and C. Masouros, "Faster-Than-Nyquist Symbol-Level Precoding for Wideband Integrated Sensing and Communications," *arXiv preprint arXiv:2306.14509*, 2023.

[19] Z. Zhang, Q. Chang, F. Liu, and S. Yang, "Dual-Functional Radar-Communication Waveform Design: Interference Reduction Versus Exploitation," *IEEE Commun. Lett.*, vol. 26, no. 1, pp. 148–152, 2022.

[20] M. Wang and H. Du, "Symbol-Level Precoding Design for Integrated Sensing and Communication," in *2022 IEEE 8th International Conference on Computer and Communications (ICCC)*, 2022, pp. 967–971.

[21] E. Björnson, E. Jorswieck *et al.*, "Optimal resource allocation in coordinated multi-cell systems," *Foundations and Trends® in Communications and Information Theory*, vol. 9, no. 2–3, pp. 113–381, 2013.

[22] C. Masouros and G. Zheng, "Exploiting Known Interference as Green Signal Power for Downlink Beamforming Optimization," *IEEE Trans. on Signal processing*, vol. 63, no. 14, pp. 3628–3640, 2015.

[23] A. Li, D. Spano, J. Krivochiza, S. Domouchtsidis, C. G. Tsinos, C. Masouros, S. Chatzinotas, Y. Li, B. Vucetic, and B. Ottersten, "A Tutorial on Interference Exploitation via Symbol-Level Precoding: Overview, State-of-the-Art and Future Directions," *IEEE Commun. Surveys & Tutorials*, vol. 22, no. 2, pp. 796–839, 2020.

[24] Z. Wei, R. Xu, Z. Feng, H. Wu, N. Zhang, W. Jiang, and X. Yang, "Symbol-level integrated sensing and communication enabled multiple base stations cooperative sensing," *IEEE Transactions on Vehicular Technology*, 2023.

[25] X. Wang, H. Wu, Y. Xu, H. Cao, N. Kumar, and J. J. Rodrigues, "Resource Allocation in Multi-Cell Integrated Sensing and Communication Systems: A DRL Approach," in *ICC 2023-IEEE International Conference on Communications*. IEEE, 2023, pp. 3210–3215.

[26] R. Li, Z. Xiao, and Y. Zeng, "Beamforming Towards Seamless Sensing Coverage for Cellular Integrated Sensing and Communication," in *2022 IEEE International Conference on Communications Workshops (ICC Workshops)*. IEEE, 2022, pp. 492–497.

[27] Y. Xu, L. Xie, D. Xu, and S. Song, "Fundamental Limits and Base Station Selection for Collaborative Sensing in Perceptive Mobile Networks," in *2023 IEEE International Mediterranean Conference on Communications and Networking (MeditCom)*. IEEE, 2023, pp. 97–102.

[28] D. Xu, A. Khalili, X. Yu, D. W. K. Ng, and R. Schober, "Integrated Sensing and Communication in Distributed Antenna Networks," *arXiv preprint arXiv:2210.14880*, 2022.

[29] D. Xu, C. Liu, S. Song, and D. W. K. Ng, "Integrated Sensing and Communication in Coordinated Cellular Networks," *arXiv preprint arXiv:2305.01213*, 2023.

[30] Y. Xu, D. Xu, L. Xie, and S. Song, "Joint BS Selection, User Association, and Beamforming Design for Network Integrated Sensing and Communication," *arXiv preprint arXiv:2305.05265*, 2023.

[31] W. Jiang, Z. Wei, F. Liu, Z. Feng, and P. Zhang, "Collaborative Precoding Design for Adjacent Integrated Sensing and Communication Base Stations," *arXiv preprint arXiv:2310.08246*, 2023.

[32] X. Liu, H. Zhang, K. Long, A. Nallanathan, and V. C. Leung, "Distributed Unsupervised Learning for Interference Management in Integrated Sensing and Communication Systems," *IEEE Transa. on Wireless Commun.*, 2023.

[33] J. Zhang, Z. Fei, X. Wang, P. Liu, J. Huang, and Z. Zheng, "Joint Resource Allocation and User Association for Multi-Cell Integrated Sensing and Communication Systems," *EURASIP Journal on Wireless Communications and Networking*, vol. 2023, no. 1, p. 64, 2023.

[34] N. Babu and C. Masouros, "Multi-cell Coordinated Joint Sensing and Communications," in *2023 Asilomar Conference*. IEEE, 2023.

[35] Z. Wei, C. Masouros, K.-K. Wong, and X. Kang, "Multi-cell interference exploitation: Enhancing the power efficiency in cell coordination," *IEEE Transactions on Wireless Communications*, vol. 19, no. 1, pp. 547–562, 2019.

[36] M. Benzaghta, G. Geraci, D. Lopez-Perez, and A. Valcarce, "Designing Cellular Networks for UAV Corridors via Bayesian Optimization," *arXiv preprint arXiv:2308.05052*, 2023.

[37] J. Li, L. Xu, P. Stoica, K. W. Forsythe, and D. W. Bliss, "Range Compression and Waveform Optimization for MIMO Radar: A Cramér–Rao Bound Based Study," *IEEE Trans. on Signal Processing*, vol. 56, no. 1, pp. 218–232, 2007.

[38] M. Grant and S. Boyd, "CVX: Matlab Software for Disciplined Convex Programming, version 2.1," 2014.

[39] K. L. Law and C. Masouros, "Symbol Error Rate Minimization Precoding for Interference Exploitation," *IEEE Transactions on Communications*, vol. 66, no. 11, pp. 5718–5731, 2018.

[40] J. C. Bezdek and R. J. Hathaway, "Convergence of Alternating Optimization," *Neural, Parallel & Scientific Computations*, vol. 11, no. 4, pp. 351–368, 2003.

[41] H. Jiang, T. Kathuria, Y. T. Lee, S. Padmanabhan, and Z. Song, "A Faster Interior Point Method for Semidefinite Programming," in *2020 IEEE 61st annual symposium on foundations of computer science (FOCS)*. IEEE, 2020, pp. 910–918.

[42] A. Li, F. Liu, X. Liao, Y. Shen, and C. Masouros, "Symbol-level precoding made practical for multi-level modulations via block-level rescaling," in *2021 IEEE 22nd International Workshop on Signal Processing Advances in Wireless Communications (SPAWC)*. IEEE, 2021, pp. 71–75.